PERGAMON

International Journal of Solids and Structures 39 (2002) 6159–6190

INTERNATIONAL JOURNAL OF SOLIDS and STRUCTURES

www.elsevier.com/locate/ijsolstr

Electro-chemo-mechanical couplings in swelling clays derived from a micro/macro-homogenization procedure

Christian Moyne [a], Márcio A. Murad [b,*]

[a] *LEMTA CNRS–INPL–UHP (UMR 7563), 2, avenue de la Forêt de Haye, 54504 Vandœuvre lès Nancy Cedex, France*
[b] *Laboratório Nacional de Computação Científica LNCC/MCT, Av Getúlio Vargas 333, 25651-070 Petrópolis, RJ, Brazil*

Received 3 October 2001; received in revised form 24 July 2002

Abstract

A macroscopic model for highly compacted expansive clays composed of a charged solid phase saturated by a binary monovalent aqueous electrolyte solution is derived based on a rigorous scale-up of the microstructural behavior. The homogenization technique is applied to propagate information available in the pore-scale model to the macroscale. Macroscopic electrokinetic phenomena such as electro-osmotic flow driven by streaming potential gradients, electrophoretic motion of mobile charges and osmotically induced swelling are derived by homogenizing the microscopic electro-hydrodynamics coupled with the Nernst–Planck and Poisson–Boltzmann equations governing the flow of the electrolyte solution, ion movement and electric potential distribution. A notable consequence of the upscaling procedure proposed herein are the micromechanical representations for the electrokinetic coefficients and swelling pressure. The two-scale model is discretized by the finite element method and applied to numerically simulate contaminant migration and electrokinetic attenuation through a compacted clay liner underneath a sanitary landfill.

Keywords: Swelling clay; Homogenization; Streaming potential; Soil liner; Poisson–Boltzmann; Electro-osmosis; Chemico-osmosis; Electrophoresis; Double-layer theory; Modified Terzaghi's principle; Disjoining (swelling) pressure

1. Introduction

Electrochemical interaction between colloidal particles and an aqueous solution is a central subject in colloid science. This phenomenon is typical of expansive media including clays, shales, polymers gels, corneal endothelium and connective biological tissues. Clay minerals are extensively used in a wide range of applications. They are a key component in the formulation of ceramic products and drilling fluids. They are widely distributed in the earth's crust and play a crucial role in many aspects of nutrition on earth. Swelling of smectitic clay soils also have undesired consequences when they heave upward upon hydration (or shrink upon desication) causing damage to the foundations of buildings. Shales have been responsible for many wellbore instability problems. Due to their low hydraulic conductivity, plasticity, swelling and adsorptive

* Corresponding author. Tel.: +55-2-4233-6149; fax: +55-2-4233-6165.
E-mail addresses: christian.moyne@ensem.inpl-nancy.fr (C. Moyne), murad@lncc.br (M.A. Murad).

0020-7683/02/$ - see front matter
PII: S0020-7683(02)00461-4

capacity for contaminants, bentonitic based compacted clays have been used as sealing materials to inhibit the migration of contaminants to the environment. In order to understand the effects of the complex physico-chemical interaction of compounds with the clay surface and their correlation with the macroscopic response of the clay buffer it becomes essential to develop accurate macroscopic constitutive models capable of capturing and representing in an averaged fashion the intriguing and challenging microscopic features inherent to the physical–chemical interactions between the macromolecules and interlayer water.

Each smectitic clay mineral is a 2:1 layer composed of an octahedral aluminia sheet sandwiched between two silica tetrahedral sheets forming an unit layer. The units are stacked together to form what is known as the crystal lattice. An important property inherent to many colloidal clay minerals is the negative charge of their surface which is a consequence of the isomorphous substitutions of certain atoms of their structure and the presence of imperfections within the interior of the crystal lattice. The negative potential is compensated by the adsorption of cations on the surface forming the inner compact layer commonly referred to as the immobile Stern layer. Nevertheless the majority of the excess of positively charged counter-ions are located in the electrolyte aqueous solution externally to the crystal forming an outer diffuse layer composed of mobile charges. Together with the fixed charged groups of the solid matrix these ions form the so-called electrical double layer (e.d.l.). The equilibrium structure of completely dissociated electrolytes around the colloids is calculated by classical electrostatics, where charge distribution and electrical field are governed by a Poisson–Boltzmann equation (see e.g. Hunter, 1994; Olphen, 1977).

When advected by the streaming velocity of the fluid, the excess in mobile charge population in the counter-ion atmosphere leads to macroscopic observed electrokinetic phenomena such as streaming currents, resulting from the influence of fluid movement upon charge flow. Moreover, to conserve charge, the movement of the net charge generates an electric potential, often referred to as streaming potential, which gives rise to other macroscopic electrokinetic phenomena. The spatial variability of this quantity engenders electrophoretic movement to the mobile charges inducing a conduction Ohmic current which opposes the streaming current and consequently slows down the counter-ions of the diffuse double layer. Due to the viscous drag interaction, the ions pull the liquid with them resulting in a concomitant electro-osmotic seepage flow opposing the pressure-gradient driven flow. This electrokinetic coupling has been commonly referred to as the electro-viscous effect as its overall influence upon the flow is usually treated through an increase in the viscosity of the liquid (see e.g. Ren et al., 2001; Hunter, 1981; Sherwood et al., 2000). In addition to electrokinetic phenomena, flow driven by chemical-osmotic effects (gradient of the Nernst potential) is also manifested particularly when the salinity varies spatially (Gu et al., 1998a).

Electrokinetic and chemical-osmotic effects are also manifested in the appearance of physico-chemical stresses in the solid phase which cause the expansion/shrinking of the clay lattice. When dry smectite is placed in a moist atmosphere, the montmorillonite superimposed layers are available for hydration and cation exchange by uptaking water in the interlayer. Swelling is the moving apart or disjoining of the clay particles until they reach their equilibrium separation under a certain overburden pressure (Derjaguin et al., 1987; Israelachvili, 1991). Macroscopically, the overburden pressure that must be applied to a saturated mixture of clay and interlayer water to keep the layers from moving apart is the experimentally observed swelling pressure (Low, 1987).

During the past few decades a significant amount of research has been developed toward the derivation of models capable of capturing coupled electro-chemo-hydro-mechanical effects in expansive porous media. In addition to the classical phenomenological approaches developed at the macroscale (see e.g. Philip, 1969; Smiles and Rosenthal, 1968; Kim et al., 1992), coupling phenomena can naturally be described within the framework of the Mixture Theory and Thermodynamics of Irreversible Processes. In this approach, the interaction between matter flux, electric charge and chemical osmosis are typical phenomena which can be properly embedded in the framework of Onsager's reciprocity relations (see e.g. Lai et al., 1991; Huyghe and Janssen, 1997; Gu et al., 1998a,b; Heidug and Wong, 1996; Hueckel, 1992b; Murad, 1999; Mow et al., 1998; Levenston et al., 1998; Bennethum et al., 2000; Zhou et al., 1998).

Despite the widespread use of non-equilibrium thermodynamics and Onsager's reciprocity relations in the macroscopic modeling of electro-chemo-mechanical coupling phenomena, to the authors knowledge very limited accomplishments have been achieved toward the incorporation of the morphology and clay microstructure in the macroscopic model. As mixture theoretic approaches are directly conducted at the macroscale, the complex microstructural solid–fluid interactions are represented in an averaged fashion by the electrokinetic coefficients whose magnitudes are usually obtained seated on experimental evidence. On the other hand it has been advocated that the clay microstructure plays a paramount importance in many physico-chemical aspects observed at the macroscale. For example, it is well known that the swelling pressure is strongly dictated by particle orientation and anisotropy (Anandarajah, 1997). Moreover, some discrepancies between the constitutive relation for the macroscopic swelling pressure and its microscale counterpart, commonly referred to as Derjaguin's disjoining pressure (Derjaguin et al., 1987) have been observed. Although this latter microscopic quantity has incorporated both chemico-osmotic and Maxwell stresses (Derjaguin et al., 1987; Dahnert and Huster, 1999), the dependence of the macroscopic swelling pressure on salt concentration has not incorporated similar effects, being commonly identified with the macroscopic osmotic pressure (see e.g. Barbour and Fredlund, 1989).

Furthermore very little information has been available to identify some of the macroscopic electrokinetic coefficients. For instance, when the porous medium is composed of a bundle of capillary tubes with diameter large compared to the thickness of the e.d.l., the electro-osmotic permeability has been identified as proportional to the zeta potential (the electric potential in the plane of shear which delimits the domains occupied by the fixed and mobile charges) in terms of the Helmholtz–Smoluchowski model (see e.g. Shang, 1997; Hunter, 1981; Coelho et al., 1996). However, very little is known on the behavior of this coefficient when the Helmholtz–Smoluchowski theory is no longer valid, for example for a random pore geometry, or even when the diameter of the tubes is of the order of the Debye's length. In this latter case extensions of the Helmholtz–Smoluchowski formula have been proposed based on empirical correction factors aiming at capturing the influence of the overlapping between the e.d.l. upon the magnitude of the electro-osmotic permeability (Hunter, 1981).

The aim of the paper is to derive a macroscopic model for compacted swelling clays capable of establishing a precise correlation between the macroscopic parameters and microscopic electro-hydrodynamics. The microscale governing equations consist of the modified Stokes flow coupled with Nernst–Planck/Poisson–Boltzmann equations (Samson et al., 1999) to describe the movement of the electrolyte solution, ion transport and local electrostatics within the fluid. Assuming local periodicity and scale separation, we then adopt the homogenization procedure (Sanchez-Palencia, 1980) to derive macroscopic equations via formal application of matched asymptotic expansion techniques. Among other effects, a notable feature of the homogenization procedure is that it provides the correct physics underlying the magnitude of each macroscopic electrokinetic parameter. Such information is carried out by solving unit cell problems which furnish knowledge on the microstructural behavior of the swelling medium. To the authors opinion, this enhanced information may be of utmost importance in providing complementary information to validate experimental data.

The two-scale model is applied to describe chemo-mechanical induced consolidation of a clay liner underneath an engineered landfill. The fully coupled non-linear macroscale model is discretized by the finite element method. Simultaneously the microscopic behavior is incorporated by solving the local unit cell problems for a given idealized stratified microstructure. The solution of the local problems is sought at each step and used to provide updated information on the macroscopic electrokinetic coefficients and swelling pressure. Numerical results illustrate the coupling between the migration of leachates through the compacted clay liner and changes in porosity and permeability due to the suppression of the e.d.l. within the fine structure as the concentration of the contaminant increases in time. Further, numerical results also illustrate the effects of the electro-osmotic attenuation upon fluid flow which is depicted in terms of the spatial variations of the streaming potential.

2. Microscopic model

At the microscale we consider an uniformly negatively charged compacted montmorillonite saturated by a continuum dielectric aqueous solution with binary symmetric electrolytes Na^+ and Cl^-. The solvent is considered a dilute solution with the ions treated as point particles at infinite dilution such that steric and hydration effects are neglected. In what follows we begin by presenting the micromechanical model developed in Moyne and Murad, 1999, in press governing fluid flow, ion transport, electric potential distribution and particle deformation. Subsequently, we exploit a decomposition of the electric potential proposed in Sasidhar and Ruckenstein (1981, 1982) and Bike and Prieve (1992) which leads to the appearance of the streaming potential. We then exploit this decomposition and rephrase the governing equations in a more appropriate form which is capable of capturing phenomena driven by streaming potential gradients, such as macroscopic electro-osmostic flow in Darcy's law and the electrophoretic migration of the ions.

2.1. Electrostatics

Let Ω_f and Ω_s be the microscopic domains occupied by the fluid and solid and let Γ denote the common interface. Further let $\{c^+, c^-\}$ and $\{\Phi, \boldsymbol{E}\}$ designate the pairs of molar concentrations of cations/anions and electric potential/electric field respectively. In classical electrostatics Φ and $\boldsymbol{E}$ are governed by the Poisson problem (see e.g. Landau and Lifshitz, 1960)

$$\begin{cases} \tilde{\varepsilon}\tilde{\varepsilon}_0 \nabla \cdot \boldsymbol{E} = q, \\ \boldsymbol{E} = -\nabla\Phi \quad \text{in } \Omega_f, \end{cases} \tag{1}$$

where $\tilde{\varepsilon}_0$ and $\tilde{\varepsilon}$ are the vacuum permittivity and the relative dielectric constant of the solvent and q is the net charge density. Denoting F and z the Faraday constant and the valence ($z = z_+ = -z_-$ for symmetrical covalent electrolytes), by definition q is the product between the molar charge and the concentration difference between cations and anions, i.e. $q \equiv zF(c^+ - c^-)$.

2.2. Modified stokes problem

Assuming the electrolyte solution incompressible and newtonian, the viscous flow is perturbed by a body force term of Coulomb type $q\boldsymbol{E}$ which governs locally the viscous interaction between the ions and the fluid (see e.g. Eringen and Maugin, 1989). Denoting μ_f, $\mathbf{v}$ and p the viscosity, velocity and thermodynamic pressure, the modified Stokes problem reads

$$\begin{aligned} &\mu_f \triangle \mathbf{v} - \nabla p = -q\boldsymbol{E} = q\nabla\Phi, \\ &\nabla \cdot \mathbf{v} = 0 \quad \text{in } \Omega_f, \end{aligned} \tag{2}$$

where gravity, convective and inertial effects have been neglected. The above momentum balance can also be rephrased in terms of the Cauchy stress tensor of the electrolyte solution $\boldsymbol{\sigma}_f$ as

$$\begin{aligned} &\nabla \cdot \boldsymbol{\sigma}_f = 0 \quad \text{in } \Omega_f, \\ &\boldsymbol{\sigma}_f = -p\boldsymbol{I} + 2\mu_f \mathscr{E}(\mathbf{v}) + \boldsymbol{\tau}_M, \end{aligned} \tag{3}$$

where $\boldsymbol{I}$ is the unit tensor, $\mathscr{E}(\mathbf{v})$ the symmetrical part of $\nabla\mathbf{v}$ and $\boldsymbol{\tau}_M$ is the Maxwell stress tensor (Landau and Lifshitz, 1960)

$$\boldsymbol{\tau}_M \equiv \frac{\tilde{\varepsilon}\tilde{\varepsilon}_0}{2}\left(2\boldsymbol{E} \otimes \boldsymbol{E} - E^2\boldsymbol{I}\right) \tag{4}$$

with $\otimes$ denoting the tensorial product between vectors. From (1) and (4) one may easily note that $\nabla \cdot \boldsymbol{\tau}_{\mathrm{M}} = q\boldsymbol{E}$.

2.3. Movement of the ions

Denote $\mathscr{D}_{\pm}$ the binary water–ions diffusion coefficients, T the absolute temperature (assumed constant) and R the universal ideal gas constant. The convection–diffusion equations governing ion transport are

$$\frac{\partial c^{\pm}}{\partial t} + \nabla \cdot (c^{\pm}\mathbf{v}) - \nabla \cdot \left(\frac{D_{\pm} c^{\pm}}{RT} \nabla \mu^{\pm} \right) = 0, \tag{5}$$

where μ^{+} and μ^{-} are the molar electrochemical potentials of cations and anions which under the dilute solution approximation are given as (see e.g. Callen, 1985; Lyklema, 1993)

$$\mu^{\pm} \equiv \pm zF\Phi + RT \log c^{\pm}. \tag{6}$$

Denoting $\overline{\Phi} = F\Phi/RT$ the dimensionless electric potential and assuming monovalent ions ($z = 1$), from (6) we have

$$\frac{1}{RT} \nabla \mu^{\pm} = \frac{\nabla c^{\pm}}{c^{\pm}} \pm \nabla \overline{\Phi}. \tag{7}$$

Further, using (7) in (5) we obtain the Nernst–Planck equation (Samson et al., 1999)

$$\frac{\partial c^{\pm}}{\partial t} + \nabla \cdot (c^{\pm}\mathbf{v}) = \nabla \cdot \left[\mathscr{D}_{\pm} \left(\nabla c^{\pm} \pm c^{\pm} \nabla \overline{\Phi} \right) \right] = \nabla \cdot \left[\mathscr{D}_{\pm} \exp(\mp \overline{\Phi}) \nabla \left(c^{\pm} \exp(\pm \overline{\Phi}) \right) \right]. \tag{8}$$

The r.h.s. of (8) shows that ion diffusion is governed by the sum of a Fickian term and an electrophoretic component which governs the movement of the ions under the effects of the electric field.

2.4. Deformation of the solid particles

Assume that the clay particles are linear elastic and isotropic with Lamé constants λ_{s} and μ_{s}. Denoting $\boldsymbol{u}$ and $\boldsymbol{\sigma}_{\mathrm{s}}$ the displacement and stress tensor of the clay particles, the classical elasticity problem reads

$$\begin{aligned} &\nabla \cdot \boldsymbol{\sigma}_{\mathrm{s}} = 0 \quad \text{in } \Omega_{\mathrm{s}}, \\ &\boldsymbol{\sigma}_{\mathrm{s}} = \lambda_{\mathrm{s}} \nabla \cdot \boldsymbol{u} \boldsymbol{I} + 2\mu_{\mathrm{s}} \mathscr{E}(\boldsymbol{u}). \end{aligned} \tag{9}$$

2.5. Boundary conditions

Denote $\boldsymbol{n}$ the unit normal exterior to Ω_{f} and let $\sigma < 0$ be the fixed surface charge of the solid particles. Considering Γ an impervious solid–fluid interface, together with the no-slip condition, continuity of the normal component of the stress tensor, and the relation between the electric field and surface charge density we have the following boundary conditions

$$\begin{aligned} &D_{\pm} c^{\pm} \nabla \mu^{\pm} \cdot \boldsymbol{n} = 0, \qquad \mathbf{v} = \frac{\partial \boldsymbol{u}}{\partial t} \quad \text{on } \Gamma, \\ &\boldsymbol{\sigma}_{\mathrm{s}} \boldsymbol{n} = \boldsymbol{\sigma}_{\mathrm{f}} \boldsymbol{n}, \qquad \tilde{\varepsilon} \tilde{\varepsilon}_0 \boldsymbol{E} \cdot \boldsymbol{n} = -\sigma, \end{aligned} \tag{10}$$

where σ and q are related through the overall electroneutrality condition

$$\int_{\Omega_{\mathrm{f}}} q \, \mathrm{d}\Omega_{\mathrm{f}} = \tilde{\varepsilon} \tilde{\varepsilon}_0 \int_{\Omega_{\mathrm{f}}} \nabla \cdot \boldsymbol{E} \, \mathrm{d}\Omega_{\mathrm{f}} = \tilde{\varepsilon} \tilde{\varepsilon}_0 \int_{\Gamma} \boldsymbol{E} \cdot \boldsymbol{n} \, \mathrm{d}\Gamma = - \int_{\Gamma} \sigma \, \mathrm{d}\Gamma. \tag{11}$$

3. Alternative microscale formulation

By invoking the classical results of electrokinetics governing flow and charge transport in capillary tubes (see e.g. Gross and Osterlé, 1968; Fair and Osterlé, 1971; Sasidhar and Ruckenstein, 1981, 1982; Yang and Li, 1998) and comparing them with the corresponding equilibrium results of the e.d.l. theory (Olphen, 1977; Hunter, 1994) one may note that variables such as Φ, $\boldsymbol{E}$, p and $c^{\pm}$ incorporate quantities of completely different nature. For example, the fluid pressure/electric potential $\{p, \Phi\}$ incorporate the bulk phase pressure/streaming potential (which are inherent to the bulk solution) and Donnan osmotic pressure/e.d.l. potential which are properties typically associated with the e.d.l. The former pair varies slowly with the fluid flow whereas the latter varies strongly across the pore even at equilibrium. Thus, the preceding micromechanical description can be enhanced if we decompose these variables into "slow" and "fast" components and reformulate the local description in terms of the decomposed quantities.

3.1. Streaming potential and bulk concentration

Following the approach proposed in Sasidhar and Ruckenstein (1981, 1982) and Bike and Prieve (1992) in order to split the effects in the electric potential which arise from typical e.d.l. and those induced from fluid flow, we write Φ in the form

$$\Phi = \varphi + \psi. \tag{12}$$

To characterize φ and ψ, the former aims at representing a potential which varies across the pore domain, purely related to double layer effects, whereas the latter component is selected to play a similar role of the so-called *streaming potential* which develops in order to maintain electroneutrality (Yang and Li, 1998; Sasidhar and Ruckenstein, 1981). We then characterize ψ as an electric potential inherent to the species of a bulk solution which is constructed locally at thermodynamic equilibrium with ions. Denote c_{b} the concentration associated with the local bulk solution (same for both co-ions and counterions) and define $\mu_{\mathrm{b}}^{\pm} \equiv \pm F\psi + RT \log c_{\mathrm{b}}$ the corresponding electrochemical potential, which by construction is given as $\mu_{\mathrm{b}}^{\pm} \equiv \mu^{\pm}$. Note that rather than non-ionic, a streaming potential ψ is assigned to the bulk solution and the characterization of c_{b} relies in the absence of the excess of one component relative to the other ($c_{\mathrm{b}}^{+} = c_{\mathrm{b}}^{-} = c_{\mathrm{b}}$) and in the consequent absence of a net charge density ($q_{\mathrm{b}} \equiv F(c_{\mathrm{b}}^{+} - c_{\mathrm{b}}^{-}) = 0$).

Introducing the dimensionless quantities $\overline{\varphi} \equiv F\varphi/RT$ and $\overline{\psi} \equiv F\psi/RT$ and using (6) (with $z = 1$), the equality between the chemical potentials furnishes

$$\mu_{\mathrm{b}}^{\pm} \equiv \pm F\psi + RT \log c_{\mathrm{b}} = \mu^{\pm} = \pm F\Phi + RT \log c^{\pm}$$

in which along with (12) leads to the following generalized Boltzmann distributions

$$c^{\pm} = c_{\mathrm{b}} \exp(\mp\overline{\Phi} \pm \overline{\psi}) = c_{\mathrm{b}} \exp(\mp\overline{\varphi}), \qquad q = -2Fc_{\mathrm{b}} \sinh \overline{\varphi}. \tag{13}$$

An important consequence of (13) is the extension of the Boltzmann distributions to the non-equilibrium case by subtracting ψ from the overall potential Φ. Thus, the spatial distribution of ψ assigns reference values of the electric potential to which the excess $\varphi = \Phi - \psi$ plays the role of a potential purely associated with e.d.l. effects. In contrast to φ, the streaming potential is tied up directly to the macroscopic flow and transport processes and to the enforcement of the electroneutrality condition.

3.2. Auxiliary concentrations

The Nernst–Planck model (8) can also be represented in terms of classical non-linear convection–diffusion equations (in the absence of the electrophoretic term due to $\nabla\overline{\Phi}$) by simply adopting a change in variables and making use of auxiliary concentrations. In a similar fashion to the bulk concentration c_{b} these

auxiliary variables, denoted by c_{f}^{+} and c_{f}^{-}, are introduced as "fictitious" NaCl concentrations in a non-ionic solution which are constructed locally at equilibrium with cations and anions i.e. with the same electrochemical potential. The relations between $c^{\pm}$ and $c_{\mathrm{f}}^{\pm}$ can be derived by defining the chemical potentials of the neutral species $\mu_{\mathrm{f}}^{\pm} \equiv RT \log c_{\mathrm{f}}^{\pm}$ (Callen, 1985). By construction and using definition (6) (with $z = 1$), the local equilibrium conditions $\mu_{\mathrm{f}}^{\pm} = \mu^{\pm}$ give

$$RT \log c_{\mathrm{f}}^{\pm} = \pm F\Phi + RT \log c^{\pm}$$

which implies in the local Boltzmann transformations for $c_{\mathrm{f}}^{\pm}$

$$c_{\mathrm{f}}^{+} \equiv c^{+} \exp(\overline{\Phi}), \quad c_{\mathrm{f}}^{-} \equiv c^{-} \exp(-\overline{\Phi}) \quad c_{\mathrm{f}}^{\pm} = c_{\mathrm{b}} \exp(\pm\overline{\psi}). \tag{14}$$

Hence, $c_{\mathrm{f}}^{\pm} = c^{\pm}$ when $\Phi = 0$ which characterizes $c_{\mathrm{f}}^{\pm}$ as concentrations of non-ionic species at local thermodynamic equilibrium with the ions. Using (14) in (8) and in boundary condition (10)(a) we obtain that $c_{\mathrm{f}}^{\pm}$ are governed by

$$\frac{\partial}{\partial t}\left[\exp(\mp\overline{\Phi})c_{\mathrm{f}}^{\pm}\right] + \nabla \cdot \left[\exp(\mp\overline{\Phi})c_{\mathrm{f}}^{\pm}\mathbf{v}\right] = \nabla \cdot \left(D_{\pm} \exp(\mp\overline{\Phi})\nabla c_{\mathrm{f}}^{\pm}\right) \tag{15}$$

along with the homogeneous Neumann condition $D_{\pm} \exp(\mp\overline{\Phi})\nabla c_{\mathrm{f}}^{\pm} \cdot \boldsymbol{n} = 0$ on Γ. As we shall illustrate next, due to the resemblance with classical convection–diffusion equations, the above form is more convenient to homogenize (Auriault and Adler, 1995). Conversely, we have characterized a "true" bulk solution by the absence of excess of one species relative to another, i.e. in a bulk solution $c_{\mathrm{f}}^{+} = c_{\mathrm{f}}^{-} = c_{\mathrm{f}}$ which leads to the absence of a net charge density ($q_{\mathrm{f}} \equiv F(c_{\mathrm{f}}^{+} - c_{\mathrm{f}}^{-}) = 0$). Clearly from (14) the concentrations $c_{\mathrm{f}}^{\pm}$ do not fulfill this requirement and therefore they correspond to hypothetical concentrations which are not associated with a bulk solution and behave discontinuously across membranes separating the electrolyte solution from an outer bulk fluid.

To summarize we then have the Boltzmann relations

$$c^{\pm} = c_{\mathrm{f}}^{\pm} \exp(\mp\overline{\Phi}) = c_{\mathrm{b}} \exp(\mp\overline{\Phi} \mp \overline{\psi}) = c_{\mathrm{b}} \exp(\mp\overline{\varphi}).$$

Finally it should be noted that for the particular case of absence of fluid flow and ion transport, when the electrolyte solution is at equilibrium which an outer saline bath of concentration c_{eq}, the classical equilibrium distributions of the e.d.l. theory shall be recovered from our results by simply setting $\overline{\psi} = cte \equiv 0$, $\overline{\Phi} = \overline{\varphi}$ and $c_{\mathrm{f}}^{\pm} = c_{\mathrm{b}} = c_{\mathrm{eq}}$.

3.3. Bulk fluid pressure

Likewise $c^{\pm}$ and Φ, the pressure p varies across the fluid domain at equilibrium and its magnitude incorporates the effects of the bulk phase pressure of the outer solution p_{b} and Donnan osmotic pressure π, which for dilute solutions is classically defined in terms of the Van't Hoff relation $\pi = RT(c^{+} + c^{-} - 2c_{\mathrm{b}})$ (Donnan, 1924; Huyghe and Janssen, 1997). Thus a decomposition similar to (12) can be adopted for p which can also be identified with a pointwise extended definition for p_{b} within the fluid phase. To accomplish this task we begin by rewriting the Coulomb term in the modified Stokes problem (2) as $-q\boldsymbol{E} = q\nabla\Phi = \nabla(\int_0^{\Phi} q(\phi)\,\mathrm{d}\phi)$. Using this result, the pressure gradient along with the Coulomb term in (2) can be rewritten as $\nabla p + q\nabla\Phi = \nabla(p + \int_0^{\Phi} q\,\mathrm{d}\phi)$ which suggests this quantity as the driving force for fluid flow. Hence, we identify this quantity with a local apparent bulk phase pressure $p_{\mathrm{b}} \equiv p + \int_0^{\Phi} q\,\mathrm{d}\phi$ which plays a similar role of the classical bulk pressure of a Stokesian fluid. To confirm this statement we show that the above definition is equivalent to subtracting the osmotic pressure π from p. In fact, using (13) in the above definition we have

$$p_{\mathrm{b}} \equiv p + \int_0^{\varphi} q\,\mathrm{d}\varphi = p - 2Fc_{\mathrm{b}} \int_0^{\varphi} \sinh\overline{\varphi}\,\mathrm{d}\varphi = p - 2RTc_{\mathrm{b}}(\cosh\overline{\varphi} - 1) = p - RT(c^{+} + c^{-} - 2c_{\mathrm{b}}) = p - \pi \tag{16}$$

which shows the desired result. Hence, likewise the bulk concentration c_{b}, the reference quantity p_{b} plays the role of the pressure of a bulk fluid constructed locally at hydrodynamic equilibrium with the electrolyte solution (this pressure has been also termed solvent pressure (see e.g. Sasidhar and Ruckenstein, 1982).

Using (12), (13) and (16), in terms of p_{b} the modified Stokes problem (2) can be rewritten as

$$\begin{aligned}\mu_{\mathrm{f}}\triangle\mathbf{v} - \boldsymbol{\nabla}p_{\mathrm{b}} - 2RT(\cosh\overline{\varphi} - 1)\boldsymbol{\nabla}c_{\mathrm{b}} &= 2RTc_{\mathrm{b}}\sinh\overline{\varphi}\boldsymbol{\nabla}\overline{\varphi} - 2Fc_{\mathrm{b}}\sinh\overline{\varphi}\boldsymbol{\nabla}\Phi \\ &= 2RTc_{\mathrm{b}}\sinh\overline{\varphi}\boldsymbol{\nabla}(\overline{\varphi} - \overline{\Phi}) = -2RTc_{\mathrm{b}}\sinh\overline{\varphi}\boldsymbol{\nabla}\overline{\psi}.\end{aligned} \tag{17}$$

4. Homogenization

In this section we adopt the homogenization procedure to upscale the microscopic problem to the macroscale. In this framework the macroscopic swelling medium is idealized as a bounded domain Ω^{ϵ} with a periodic structure. Following the general framework of homogenization (see e.g. Sanchez-Palencia, 1980), introduce the microscopic characteristic length-scale associated with the cell (l), for which microscopic heterogeneities are relevant, and the macroscopic length-scale related to the overall dimensions of the clay (L) where the heterogeneities are invisible. Define the perturbation parameter as the ratio $\epsilon \equiv l/L$. Make use of the scale separation assumption wherein the characteristic length l is small in comparison with the macroscopic length scale L such that $\epsilon \ll 1$. Consider Ω^{ϵ} composed of spatially repeated unit disjoint parallelepiped periods, Y^{ϵ}, congruent to a standard Y formed by the union of cell domains Y_{s} and Y_{f} occupied by the clay particles and electrolyte solution respectively. Denote $\Omega^{\epsilon}_{\mathrm{f}}$ and $\Omega^{\epsilon}_{\mathrm{s}}$ the fluid and solid subdomains of Ω^{ϵ} given by the union of cell domains ϵY_{f} and ϵY_{s} respectively whereas the interface Γ^{ϵ} is given by the union of $\partial(\epsilon Y_{\mathrm{fs}})$ interfaces. Our starting point, $\epsilon = 1$, corresponds to our microscopic model. The ϵ-model in Ω^{ϵ} consists of properly scaled equations on a lattice of copies ϵY. In order to determine a macroscopic equivalent description, the asymptotic behavior of the periodic solution of the microscopic equations is sought as the scale of the inhomogeneity decays asymptotically when the parameter $\epsilon \to 0$.

4.1. Order of magnitude of the coefficients

An essential feature inherent to any upscaling technique is the proper scaling of the dimensionless quantities which appear in the microscopic description (Auriault, 1991). In order to establish the order of magnitude of each coefficient we begin by rewriting the micromodel in dimensionless form and then we estimate the set of non-dimensional numbers which characterize the local description. Begin by assigning the subscript "ref" to the reference value for which the corresponding microscopic quantity is normalized. The reference characteristic length ℓ_{ref} is chosen of the order of the macroscopic medium, i.e. $\ell_{\mathrm{ref}} \equiv L$ such that the macroscopic length L is used to normalize the spatial differential operators. Likewise, the time scale is normalized with respect to $t_{\mathrm{ref}} = L^2/\mathscr{D}_{\pm}$. The orders of magnitude of the reference velocity v_{ref} and pressure p_{ref} are based on classical dimensional analysis of Darcy's law which shows $v_{\mathrm{ref}} = \ell^2 p_{\mathrm{ref}}/\mu_{\mathrm{f}}L$ (Auriault, 1991). The choice of the reference electric field E_{ref} is based on boundary condition (10)(d) which suggests $E_{\mathrm{ref}} \equiv \sigma/\tilde{\varepsilon}\tilde{\varepsilon}_0$. Furthermore, since Φ and $\boldsymbol{E}$ are locally related by (1), choose $\Phi_{\mathrm{ref}} = \ell E_{\mathrm{ref}}$. The choice of the reference concentration c_{ref} is based on the electroneutrality condition (11). Since the volume integral of the net charge $q = F(c^{+} - c^{-})$ is neutralized by the surface integral of the charge density σ, the concentrations vary $1/\ell$ faster than the surface charge density and thus we select $c_{\mathrm{ref}} = \sigma/(F\ell)$. The selection of

the reference displacement of the solid phase u_{ref} is based on (10)(c) expressing continuity of the normal component of the stress tensor on Γ. Denoting $C^E_{\mathrm{ref}} \equiv 0.5\tilde{\varepsilon}\tilde{\varepsilon}_0 E^2_{\mathrm{ref}}$ the reference quantity for the Maxwell stress tensor, using the constitutive equations for the stress tensors (3) and (9) and the relation between v_{ref} and p_{ref}, we choose $(\lambda_{\mathrm{s}} + 2\mu_{\mathrm{s}})u_{\mathrm{ref}}/L = p_{\mathrm{ref}} + \mu_{\mathrm{f}} v_{\mathrm{ref}}/l + C^E_{\mathrm{ref}} = (1+\epsilon)p_{\mathrm{ref}} + C^E_{\mathrm{ref}} \approx p_{\mathrm{ref}} + C^E_{\mathrm{ref}}$. Thus, by rephrasing the microscopic system in dimensionless form, the following dimensionless quantities naturally appear

$$Pe = \frac{v_{\mathrm{ref}} L}{\mathscr{D}_{\pm}}, \quad N = \frac{F\sigma\ell}{\tilde{\varepsilon}\tilde{\varepsilon}_0 RT}, \quad M_1 = \frac{\sigma^2}{\tilde{\varepsilon}\tilde{\varepsilon}_0 p_{\mathrm{ref}}}, \quad M_2 = \frac{\tilde{\varepsilon}\tilde{\varepsilon}_0 E^2_{\mathrm{ref}} L}{2u_{\mathrm{ref}}(3\lambda_{\mathrm{s}} + 2\mu_{\mathrm{s}})}.$$

The number Pe is the classical Péclet number which measures the ratio between convective and diffusive effects. The number N quantifies the ratio between the electrical and thermal molar energies (which are of the same order of magnitude) whereas the parameters M_1 and M_2 measure the magnitude of Maxwell stresses relative to the fluid pressure p in the constitutive equation (3) for $\boldsymbol{\sigma}_{\mathrm{f}}$ (recall that $\sigma^2/(\tilde{\varepsilon}\tilde{\varepsilon}_0) = \tilde{\varepsilon}\tilde{\varepsilon}_0 E_{\mathrm{ref}}$) and to the stresses in the solid particles $\boldsymbol{\sigma}_{\mathrm{s}}$ in boundary condition (10)(c). From the conventional e.d.l. theory, Maxwell stresses counterbalance the variations in osmotic pressure in the fluid domain (Derjaguin et al., 1987) and therefore the magnitude of the components of $\boldsymbol{\tau}_{\mathrm{M}}$ is of the same order of both fluid pressure p and particle stresses $\boldsymbol{\sigma}_{\mathrm{s}}$. Finally we shall consider the case where convection effects are of lower order of magnitude compared to diffusion such that the Péclet number is assumed small. Hence we adopt the following estimates

$$Pe = \mathscr{O}(\epsilon), \quad N = \mathscr{O}(1), \quad M_1 = \mathscr{O}(1), \quad M_2 = \mathscr{O}(1).$$

We remark that the above estimate for Pe does not place any constraint in the analysis. For simplicity it can be shown, using the analysis developed in Auriault and Adler (1995), that when adopting the above estimate for Pe, ion convective-diffusive motion is characterized by only one time scale $t = L^2/D_{\pm}$ associated with the diffusion process. Likewise, the other ranges of Pe where advection effects are more pronounced can also be incorporated in the analysis by pursuing the approach proposed in Auriault and Adler (1995).

Making use of the above scaling laws for the coefficients the micromechanical model is rephrased below with a formal ϵ^n factor to indicate the order of magnitude of each term. Denoting δ_{ij} the Kronecker delta symbol and $\boldsymbol{c}_{\mathrm{s}}$ the fourth-order elastic modulus tensor of the solid phase with components $c_{ijkl} = \lambda_{\mathrm{s}}\delta_{ij}\delta_{kl} + \mu_{\mathrm{s}}(\delta_{ik}\delta_{jl} + \delta_{il}\delta_{jk})$ we then have in Ω_{f}

$$\begin{aligned}
&\epsilon^2 \triangle \Phi = -\frac{q}{\tilde{\varepsilon}\tilde{\varepsilon}_0}, \quad \boldsymbol{E} = -\epsilon \nabla \Phi, \quad c^{\pm} = c^{\pm}_{\mathrm{f}} \exp\left(\mp \overline{\Phi}\right), \quad q = F(c^+ - c^-),\\
&\nabla \cdot \boldsymbol{\sigma}_{\mathrm{f}} = 0, \qquad \boldsymbol{\sigma}_{\mathrm{f}} = -p\boldsymbol{I} + \frac{\tilde{\varepsilon}\tilde{\varepsilon}_0}{2}\left(2\boldsymbol{E}\otimes\boldsymbol{E} - E^2\boldsymbol{I}\right) + 2\epsilon^2\mu_{\mathrm{f}}\mathscr{E}(\mathbf{v}),\\
&\nabla \cdot \mathbf{v} = 0, \qquad \epsilon^2\mu_{\mathrm{f}}\triangle\mathbf{v} = \nabla p_{\mathrm{b}} + 2RT(\cosh\overline{\varphi} - 1)\nabla c_{\mathrm{b}} - 2RTc_{\mathrm{b}}\sinh\overline{\varphi}\nabla\overline{\psi},\\
&\frac{\partial}{\partial t}\left[\exp\left(\mp\overline{\Phi}\right)c^{\pm}_{\mathrm{f}}\right] + \epsilon\nabla\cdot\left[\exp\left(\mp\overline{\Phi}\right)c^{\pm}_{\mathrm{f}}\mathbf{v}\right] = \nabla\cdot\left(D_{\pm}\exp\left(\mp\overline{\Phi}\right)\nabla c^{\pm}_{\mathrm{f}}\right)
\end{aligned} \tag{18}$$

and in Ω_{s}

$$\nabla\cdot\boldsymbol{\sigma}_{\mathrm{s}} = 0, \qquad \boldsymbol{\sigma}_{\mathrm{s}} = \boldsymbol{c}_{\mathrm{s}}\mathscr{E}(\boldsymbol{u})$$

and on the fluid–solid interface Γ

$$\epsilon\nabla\Phi\cdot\boldsymbol{n} = \frac{\sigma}{\tilde{\varepsilon}\tilde{\varepsilon}_0}, \quad \mathbf{v} = \frac{\partial\boldsymbol{u}}{\partial t}, \quad D_{\pm}\exp\left(\mp\overline{\Phi}\right)\nabla c^{\pm}_{\mathrm{f}}\cdot\boldsymbol{n} = 0,$$

$$\boldsymbol{\sigma}_{\mathrm{f}}\boldsymbol{n} = \left(-p\boldsymbol{I} + \frac{\tilde{\varepsilon}\tilde{\varepsilon}_0}{2}\left(2\boldsymbol{E}\otimes\boldsymbol{E} - E^2\boldsymbol{I}\right) + 2\epsilon^2\mu_{\mathrm{f}}\mathscr{E}(\mathbf{v})\right)\boldsymbol{n} = \boldsymbol{\sigma}_{\mathrm{s}}\boldsymbol{n} = \boldsymbol{c}_{\mathrm{s}}\mathscr{E}(\boldsymbol{u})\boldsymbol{n}.$$

It should be noted that at the microscale, electrical effects in the electrolyte solution induce stresses in the solid phase through the Maxwell component in the above traction boundary condition.

4.2. Matched asymptotic expansions

Following the usual framework of homogenization begin by introducing microscopic and macroscopic coordinates associated with the cell ($\boldsymbol{y}$) and the overall dimensions of the swelling medium $\boldsymbol{x} = \epsilon\boldsymbol{y}$. Consider each quantity depending on both scales in the form $f = f(\boldsymbol{x}, \boldsymbol{y})$ and postulate two-scale asymptotic expansions in terms of the perturbation parameter ϵ for the set ψ^ϵ of unknowns $\{\boldsymbol{u}, \boldsymbol{\sigma}_s\}$ and $\{\boldsymbol{\sigma}_f, \mathbf{v}, p_b, \Phi, \varphi, \psi, \boldsymbol{E}, \boldsymbol{\tau}_M, c^\pm, c_f^\pm, q, \mu^\pm\}$

$$\psi^\epsilon = \psi^0 + \epsilon\psi^1 + \epsilon^2\psi^2 + \cdots \tag{19}$$

with the coefficients ψ^i spatially periodic in $\boldsymbol{y}$ over a unit cell $Y = Y_f \cup Y_s$. Insert the expansions (19) into the set of microscopic governing equations with the differential operator ∂/∂_x replaced by $\partial/\partial_x + \epsilon^{-1}\partial/\partial_y$. After a formal matching of the powers of ϵ, we obtain a recursive system of cell problems parametrized by $\boldsymbol{x}$. For the fluid in Y_f we have

$$\triangle_{yy}\Phi^0 = -\frac{q^0}{\tilde{\varepsilon}\tilde{\varepsilon}_0}, \tag{20}$$

$$\boldsymbol{E}^0 = -\nabla_y(\varphi^0 + \psi^0), \tag{21}$$

$$\Phi^0 = \varphi^0 + \psi^0, \tag{22}$$

$$\nabla_y \cdot \mathbf{v}^0 = 0, \tag{23}$$

$$\nabla_x \cdot \mathbf{v}^0 + \nabla_y \cdot \mathbf{v}^1 = 0, \tag{24}$$

$$\nabla_y \cdot \boldsymbol{\sigma}_f^0 = 0, \tag{25}$$

$$\nabla_x \cdot \boldsymbol{\sigma}_f^0 + \nabla_y \cdot \boldsymbol{\sigma}_f^1 = 0, \tag{26}$$

$$\boldsymbol{\sigma}_f^0 = -p^0\boldsymbol{I} + \boldsymbol{\tau}_M^0, \qquad \boldsymbol{\tau}_M^0 = \frac{\tilde{\varepsilon}\tilde{\varepsilon}_0}{2}\left(2\boldsymbol{E}^0 \otimes \boldsymbol{E}^0 - (E^0)^2\boldsymbol{I}\right), \tag{27}$$

$$\nabla_y p_b^0 + 2RT\left(\cosh\overline{\varphi}^0 - 1\right)\nabla_y c_b^0 - 2RTc_b^0 \sinh\overline{\varphi}^0 \nabla_y \overline{\psi}^0 = 0, \tag{28}$$

$$\mu_f \triangle_{yy}\mathbf{v}^0 = \nabla_x p_b^0 + \nabla_y p_b^1 + 2RT\left(\cosh\overline{\varphi}^0 - 1\right)\left(\nabla_x c_b^0 + \nabla_y c_b^1\right) - 2RTc_b^0 \sinh\overline{\varphi}^0\left(\nabla_x\overline{\psi}^0 + \nabla_y\overline{\psi}^1\right), \tag{29}$$

$$c^{\pm 0} = c_f^{\pm 0}\exp(\mp\overline{\Phi}^0) = c_b^0\exp(\mp\overline{\varphi}^0), \tag{30}$$

$$c_f^{\pm 0} = c_b^0\exp(\pm\overline{\psi}^0), \tag{31}$$

$$c_f^{\pm 1} = \exp(\pm\overline{\psi}^0)\left(c_b^1 \pm c_b^0\overline{\psi}^1\right), \tag{32}$$

$$q^0 = F\left(c^{+0} - c^{-0}\right) = -2Fc_b^0 \sinh\overline{\varphi}^0, \tag{33}$$

$$\mu^{\pm 0} = \pm F\Phi^0 + RT\log c^{\pm 0} = \pm F\psi^0 + RT\log c_{\mathrm{b}}^0 = RT\log c_{\mathrm{f}}^{\pm 0}, \tag{34}$$

$$\nabla_y \cdot \left[D_\pm \exp(\mp \overline{\Phi}^0) \nabla_y c_{\mathrm{f}}^{\pm 0} \right] = 0, \tag{35}$$

$$\nabla_y \cdot \left[D_\pm \exp(\mp \overline{\varphi}^0) \left(\nabla_y c_{\mathrm{b}}^0 \pm c_{\mathrm{b}}^0 \nabla_y \overline{\psi}^0 \right) \right] = 0, \tag{36}$$

$$\nabla_y \cdot \left[D_\pm \exp(\mp \overline{\Phi}^0) (\nabla_x c_{\mathrm{f}}^{\pm 0} + \nabla_y c_{\mathrm{f}}^{\pm 1}) \right] = 0, \tag{37}$$

$$\begin{aligned} \frac{\partial}{\partial t}(\exp(\mp\overline{\Phi}^0) c_{\mathrm{f}}^{\pm 0}) + \mathbf{v}^0 \cdot \nabla_y (\exp(\mp\overline{\Phi}^0) c_{\mathrm{f}}^{\pm 0}) &= \nabla_x \cdot \left[D_\pm \exp(\mp\overline{\Phi}^0)(\nabla_x c_{\mathrm{f}}^{\pm 0} + \nabla_y c_{\mathrm{f}}^{\pm 1}) \right] \\ &\quad + \nabla_y \cdot \left[D_\pm \exp(\mp\overline{\Phi}^0)(\nabla_x c_{\mathrm{f}}^{\pm 1} + \nabla_y c_{\mathrm{f}}^{\pm 2}) \mp \overline{\Phi}^1 (\nabla_x c_{\mathrm{f}}^{\pm 0} + \nabla_y c_{\mathrm{f}}^{\pm 1}) \right]. \end{aligned} \tag{38}$$

For the clay particles in Y_{s} we have

$$\nabla_y \cdot \left(\boldsymbol{c}_{\mathrm{s}} \mathscr{E}_y(\boldsymbol{u}^0) \right) = 0, \qquad \nabla_y \cdot \left[\boldsymbol{c}_{\mathrm{s}} (\mathscr{E}_y(\boldsymbol{u}^1) + \mathscr{E}_x(\boldsymbol{u}^0)) \right] = 0, \tag{39}$$

$$\nabla_x \cdot \boldsymbol{\sigma}_{\mathrm{s}}^0 + \nabla_y \cdot \boldsymbol{\sigma}_{\mathrm{s}}^1 = 0, \qquad \boldsymbol{\sigma}_{\mathrm{s}}^0 = \boldsymbol{c}_{\mathrm{s}} \left(\mathscr{E}_x(\boldsymbol{u}^0) + \mathscr{E}_y(\boldsymbol{u}^1) \right). \tag{40}$$

Finally the parametrized boundary conditions on ∂Y_{fs} are

$$\nabla_y \Phi^0 \cdot \boldsymbol{n} = \frac{\sigma}{\tilde{\varepsilon}\tilde{\varepsilon}_0}, \quad \mathbf{v}^0 = \frac{\partial \boldsymbol{u}^0}{\partial t}, \quad \mathbf{v}^1 = \frac{\partial \boldsymbol{u}^1}{\partial t}, \tag{41}$$

$$\boldsymbol{c}_{\mathrm{s}} \left(\mathscr{E}_y(\boldsymbol{u}^0) \right) \boldsymbol{n} = 0, \qquad \boldsymbol{\sigma}_{\mathrm{s}}^1 \boldsymbol{n} = \boldsymbol{\sigma}_{\mathrm{f}}^1 \boldsymbol{n}, \tag{42}$$

$$\left(-p^0 \boldsymbol{I} + \boldsymbol{\tau}_{\mathrm{M}}^0 \right) \boldsymbol{n} = \boldsymbol{c}_{\mathrm{s}} \left(\mathscr{E}_x(\boldsymbol{u}^0) + \mathscr{E}_y(\boldsymbol{u}^1) \right) \boldsymbol{n}, \tag{43}$$

$$D_\pm \exp(\mp\overline{\Phi}^0) \nabla_y c_{\mathrm{f}}^{\pm 0} \cdot \boldsymbol{n} = 0, \tag{44}$$

$$D_\pm \exp(\mp\overline{\Phi}^0) \left(\nabla_x c_{\mathrm{f}}^{\pm 0} + \nabla_y c_{\mathrm{f}}^{\pm 1} \right) \cdot \boldsymbol{n} = 0, \tag{45}$$

$$D_\pm \exp(\mp\overline{\Phi}^0) \left(\nabla_x c_{\mathrm{f}}^{\pm 1} + \nabla_y c_{\mathrm{f}}^{\pm 2} \mp \overline{\Phi}^1 \left(\nabla_x c_{\mathrm{f}}^{\pm 0} + \nabla_y c_{\mathrm{f}}^{\pm 1} \right) \right) \cdot \boldsymbol{n} = 0. \tag{46}$$

4.2.1. Non-oscillatory variables

We begin by collecting our set of "slow" variables, which are independent of the fast coordinate $\boldsymbol{y}$. From (39)(a) and (42)(a) we obtain $\boldsymbol{u}^0(\boldsymbol{x},\boldsymbol{y},t) = \boldsymbol{u}^0(\boldsymbol{x},t)$. Further from (34), (35) and boundary conditions (44) we also have $c_{\mathrm{f}}^{\pm 0}(\boldsymbol{x},\boldsymbol{y},t) = c_{\mathrm{f}}^{\pm 0}(\boldsymbol{x},t)$ and $\mu^{\pm 0}(\boldsymbol{x},\boldsymbol{y},t) = \mu^{\pm 0}(\boldsymbol{x},t)$. Moreover, by adding (34) over cations and anions we obtain $c_{\mathrm{b}}^0(\boldsymbol{x},\boldsymbol{y},t) = c_{\mathrm{b}}^0(\boldsymbol{x},t)$ and $\psi^0(\boldsymbol{x},\boldsymbol{y},t) = \psi^0(\boldsymbol{x},t)$. Finally using these two latter results in (28) also implies $\nabla_y p_{\mathrm{b}}^0 = 0 \Rightarrow p_{\mathrm{b}}^0(\boldsymbol{x},\boldsymbol{y},t) = p_{\mathrm{b}}^0(\boldsymbol{x},t)$. Thus our set of "slow" variables is $\{c_{\mathrm{b}}^0, \psi^0, \boldsymbol{u}^0, p_{\mathrm{b}}^0, c_{\mathrm{f}}^{\pm 0}, \mu^{\pm 0}\}$.

4.2.2. Local Poisson–Boltzmann

Using decomposition (22) and (33) in the Poisson equation (20) along with boundary condition (41)(a) we obtain the local cell problem

$$\begin{aligned}&\tilde{\varepsilon}\tilde{\varepsilon}_0\triangle_{yy}\varphi^0 = -q^0 = 2Fc_{\mathrm{b}}^0(\boldsymbol{x},t)\sinh\overline{\varphi}^0 \quad \text{in } Y_{\mathrm{f}},\\ &\tilde{\varepsilon}\tilde{\varepsilon}_0\nabla_y\varphi^0\cdot\boldsymbol{n} = \sigma \quad \text{on } \partial Y_{\mathrm{fs}}\end{aligned} \tag{47}$$

with q^0 and σ subject to the local electroneutrality condition

$$\int_{Y_{\mathrm{f}}} q^0\,\mathrm{d}Y = -\int_{\partial Y_{\mathrm{fs}}}\sigma\,\mathrm{d}\Gamma. \tag{48}$$

The above result shows that the Poisson–Boltzmann problem can be extended to the non-equilibrium case locally provided Φ^0 is replaced by the relative potential φ^0. Moreover, an essential feature underlying (47) is the fact that the Poisson–Boltzmann problem does not survive at the macroscale. This arises from the scaling factor ϵ^2 in the Poisson problem (18)(a) which leads to the "shrinking" of the homogenized equation as $\epsilon\to 0$. Thus, φ^0, Φ^0 and $\boldsymbol{E}^0$ are highly oscillatory quantities which depend strongly on $\boldsymbol{y}$. Notably this fact is consistent with the e.d.l. results at equilibrium where these quantities vary across the pore fluid domain (Olphen, 1977; Hunter, 1994).

4.2.3. Movement of the ions

In order to derive the macroscopic form of the ion transport equations we begin by homogenizing (37) and (38) in terms of the auxiliary salinities $c_{\mathrm{f}}^{\pm 0}$ and then rephrase the homogenized result in terms of the pair $\{c_{\mathrm{b}}^0,\overline{\psi}^0\}$ by making use of the change in variables (31). By combining (37) with boundary condition (45) along with the decomposition (22), the closure problem for $c_{\mathrm{f}}^{\pm 1}$ consists in finding the solution of the local Neumann problems

$$\begin{aligned}&\nabla_y\cdot\left[D_\pm\exp(\mp\overline{\varphi}^0)(\nabla_y c_{\mathrm{f}}^{\pm 1}+\nabla_x c_{\mathrm{f}}^{\pm 0})\right]=0 \quad \text{in } Y_{\mathrm{f}},\\ &D_\pm\exp(\mp\overline{\varphi}^0)\left(\nabla_y c_{\mathrm{f}}^{\pm 1}+\nabla_x c_{\mathrm{f}}^{\pm 0}\right)\cdot\boldsymbol{n}=0 \quad \text{on } \partial Y_{\mathrm{fs}}\end{aligned}$$

which together with (31) can be represented up to an additive function $\hat{c}^{\pm}(\boldsymbol{x},t)$

$$c_{\mathrm{f}}^{\pm 1}=\boldsymbol{f}^{\pm}(\boldsymbol{x},\boldsymbol{y},t)\cdot\nabla_x c_{\mathrm{f}}^{\pm 0}(\boldsymbol{x},t)=\boldsymbol{f}^{\pm}\left[\exp(\pm\overline{\psi}^0)\nabla_x c_{\mathrm{b}}^0(\boldsymbol{x},t)\pm c_{\mathrm{b}}^0(\boldsymbol{x},t)\exp(\pm\overline{\psi}^0)\nabla_x\overline{\psi}^0(\boldsymbol{x},t)\right], \tag{49}$$

where $\boldsymbol{f}^{\pm}$ are auxiliary Y-periodical vectorial functions satisfying the cell problems

$$\begin{aligned}&\nabla_y\cdot\left[D_\pm\exp(\mp\overline{\varphi}^0)(\nabla_y\boldsymbol{f}^{\pm}+\boldsymbol{I})\right]=0 \quad \text{in } Y_{\mathrm{f}},\\ &D_\pm\exp(\mp\overline{\varphi}^0)\left(\nabla_y\boldsymbol{f}^{\pm}+\boldsymbol{I}\right)\cdot\boldsymbol{n}=0 \quad \text{on } \partial Y_{\mathrm{fs}}.\end{aligned} \tag{50}$$

Note that since $\overline{\varphi}^0$ depends on c_{b}^0 through the local Poisson–Boltzmann problem (47), the above characteristic functions exhibit the dependence $\boldsymbol{f}^{\pm}=\boldsymbol{f}^{\pm}(\boldsymbol{y},c_{\mathrm{b}}^0)$.

To derive the homogenized form of (38) define $\langle\cdot\rangle^\alpha\equiv|Y_\alpha|^{-1}\int_{Y_\alpha}\cdot\,\mathrm{d}Y_\alpha$ $(\alpha=\mathrm{f},\mathrm{s})$ the intrinsic volume average operator over the α-portion of the unit cell Y. Also denote $n_\alpha\equiv|Y_\alpha|/|Y|$ $(\alpha=\mathrm{f},\mathrm{s})$ the volume fraction of the α-phase and $\langle\cdot\rangle\equiv|Y|^{-1}\int_{Y_\alpha}\cdot\,\mathrm{d}Y=n_\alpha\langle\cdot\rangle^\alpha$ the average operator over Y. Integrating (38) over Y and using the closure problem (49) for $c_{\mathrm{f}}^{\pm 1}$ we obtain

$$\frac{\partial}{\partial t}\left[n_{\mathrm{f}}\langle\exp(\mp\overline{\Phi}^0)\rangle^f c_{\mathrm{f}}^{\pm 0}\right]\mp c_{\mathrm{f}}^{\pm 0}\langle\exp(\mp\overline{\Phi}^0)\boldsymbol{v}^0\cdot\nabla_y\overline{\Phi}^0\rangle=\nabla_x\cdot\left[\langle\mathscr{D}_\pm\exp(\mp\overline{\Phi}^0)(\boldsymbol{I}\pm\nabla_y\boldsymbol{f}^{\pm})\rangle\nabla_x c_{\mathrm{f}}^{\pm 0}\right], \tag{51}$$

where the average of the last term in the r.h.s. of (38) vanishes using the divergence theorem along with the boundary condition (46) and the periodicity assumptions. Furthermore, using the mass balance (23) together with the divergence theorem and the no-slip boundary condition (41)(b) one can rewrite the second term in the l.h.s. of (51) as

$$\mp c_{\mathrm{f}}^{\pm 0}\langle \exp(\mp\overline{\Phi}^0)\mathbf{v}^0\cdot\nabla_y\overline{\Phi}^0\rangle = c_{\mathrm{f}}^{\pm 0}\langle \nabla_y\cdot(\exp(\mp\overline{\Phi}^0)\mathbf{v}^0)\rangle = \frac{c_{\mathrm{f}}^{\pm 0}}{|Y|}\int_{\partial Y_{\mathrm{fs}}}\exp(\mp\overline{\Phi}^0)\mathbf{v}^0\cdot\boldsymbol{n}\,\mathrm{d}\Gamma$$
$$= \frac{c_{\mathrm{f}}^{\pm 0}}{|Y|}\int_{\partial Y_{\mathrm{fs}}}\exp(\mp\overline{\Phi}^0)\frac{\partial\boldsymbol{u}^0}{\partial t}\cdot\boldsymbol{n}\,\mathrm{d}\Gamma = c_{\mathrm{f}}^{\pm 0}\frac{\partial\boldsymbol{u}^0}{\partial t}\cdot\langle\nabla_y\exp(\mp\overline{\Phi}^0)\rangle.$$

Hence, neglecting the convective effects induced by $\partial\boldsymbol{u}^0/\partial t$, the last term vanishes and consequently (51) reduces to a purely homogenized diffusion equation. Finally, to rewrite (51) in terms of the pair $\{c_{\mathrm{b}}^0,\psi^0\}$ we make use of the generalized Boltzmann transformations (31). Defining the homogenized diffusion coefficient $\boldsymbol{D}_{\pm}^{*}\equiv\langle\mathscr{D}_{\pm}\exp(\mp\overline{\varphi}^0)(\boldsymbol{I}\pm\nabla_y\boldsymbol{f}^{\pm})\rangle^f$, we have

$$\frac{\partial}{\partial t}(n_{\mathrm{f}}\langle\exp(\mp\overline{\varphi}^0)\rangle^f c_{\mathrm{b}}^0) = \nabla_x\cdot\left[\langle\mathscr{D}_{\pm}\exp(\mp\overline{\Phi}^0)(\boldsymbol{I}\pm\nabla_y\boldsymbol{f}^{\pm})\rangle\exp(\pm\overline{\psi}^0)(\nabla_x c_{\mathrm{b}}^0\pm c_{\mathrm{b}}^0\nabla_x\overline{\psi}^0)\right]$$
$$= \nabla_x\cdot\left(\langle\mathscr{D}_{\pm}\exp(\mp\overline{\varphi}^0)(\boldsymbol{I}\pm\nabla_y\boldsymbol{f}^{\pm})\rangle\nabla_x c_{\mathrm{b}}^0\pm c_{\mathrm{b}}^0\nabla_x\overline{\psi}^0\right) = \nabla_x\cdot\left[n_{\mathrm{f}}\boldsymbol{D}_{\pm}^{*}\left(\nabla_x c_{\mathrm{b}}^0\pm c_{\mathrm{b}}^0\nabla_x\overline{\psi}^0\right)\right]. \tag{52}$$

The above result is our homogenized diffusion equations with the product $n_{\mathrm{f}}\boldsymbol{D}_{\pm}^{*}$ playing the role of an effective diffusion coefficient. It should be noted that since c_{b}^0 reflects the concentration of a bulk solution at thermodynamic equilibrium with the ions, this quantity (unlike $c_{\mathrm{f}}^{\pm 0}$) behaves continuously across the interface between the electrolyte solution and an outer saline bath. Thus, (52) is the natural formulation to describe ion movement where boundary conditions can naturally be imposed. Nevertheless, we remark the usefulness of the auxiliary result (51) as it was obtained within a straightforward homogenization procedure of classical convection–diffusion equations (see e.g. Auriault and Adler, 1995). After computing $c_{\mathrm{b}}^0(\boldsymbol{x},t)$, the averaged ion concentrations $\langle c^{\pm 0}\rangle$ can be recovered within a post-processing approach considering (13) which gives $\langle c^{\pm 0}\rangle^f = c_{\mathrm{b}}^0\langle\exp(\mp\overline{\varphi}^0)\rangle^f$. This shows that the capacitance term in the l.h.s. of (52) can also be rephrased as $\partial(n_{\mathrm{f}}\langle c^{\pm 0}\rangle^f)/\partial t$ and therefore the net charge density is also given as $\langle q^0\rangle^f = -2Fc_{\mathrm{b}}^0\langle\sinh\overline{\varphi}^0\rangle^f = F(\langle c^{+0}\rangle^f - \langle c^{-0}\rangle^f)$. Further, defining the macroscopic electric current $\boldsymbol{J}^0$ as

$$\boldsymbol{J}^0 = Fn_{\mathrm{f}}\left[\boldsymbol{D}_{+}^{*}(\nabla_x c_{\mathrm{b}}^0 + c_{\mathrm{b}}^0\nabla_x\overline{\psi}^0) - \boldsymbol{D}_{-}^{*}(\nabla_x c_{\mathrm{b}}^0 - c_{\mathrm{b}}^0\nabla_x\overline{\psi}^0)\right]$$
$$= Fn_{\mathrm{f}}\left[(\boldsymbol{D}_{+}^{*}-\boldsymbol{D}_{-}^{*})\nabla_x c_{\mathrm{b}}^0 + c_{\mathrm{b}}^0(\boldsymbol{D}_{+}^{*}+\boldsymbol{D}_{-}^{*})\nabla_x\overline{\psi}^0\right] \tag{53}$$

by multiplying (52) by F, subtracting the results for cations and anions and neglecting the effects of changes in porosity upon the electric current, we obtain the macroscopic conservation of charge

$$n_{\mathrm{f}}\frac{\partial\langle q^0\rangle^f}{\partial t} + \nabla_x\cdot\boldsymbol{J}^0 = 0. \tag{54}$$

By combining the above result with the electroneutrality condition (47) and recalling that σ is time independent we obtain the divergence free constraint $\nabla_x\cdot\boldsymbol{J}^0 = 0$. Further, as we shall observe in Appendix A.4, the above result together with macroscopic homogeneous Neumann boundary conditions ($\boldsymbol{J}^0\cdot\boldsymbol{n} = 0$) may lead, in some particular stratified one-dimensional microstructures, to the stronger form of charge conservation $\boldsymbol{J}^0 = 0$.

4.2.4. Darcy's law

To derive the macroscopic form of Darcy's law governing the movement of the electrolyte solution we begin by combining the closure relations (49) for $c_{\mathrm{f}}^{\pm 1}$ with (32) to obtain

$$\nabla_y c_{\mathrm{b}}^1\pm c_{\mathrm{b}}^0\nabla_y\overline{\psi}^1 = \exp(\mp\overline{\psi}^0)\nabla_y c_{\mathrm{f}}^{\pm 1} = \nabla_y\boldsymbol{f}^{\pm}\left(\nabla_x c_{\mathrm{b}}^0\pm c_{\mathrm{b}}^0\nabla_x\overline{\psi}^0\right)$$

in which after adding and subtracting over cations and anions yield

$$2\nabla_y c_{\mathrm{b}}^1 = \nabla_y(\boldsymbol{f}^+ + \boldsymbol{f}^-)\nabla_x c_{\mathrm{b}}^0 + \nabla_y(\boldsymbol{f}^+ - \boldsymbol{f}^-)c_{\mathrm{b}}^0\nabla_x\overline{\psi}^0,$$

$$2c_{\mathrm{b}}^0\nabla_y\overline{\psi}^1 = \nabla_y(\boldsymbol{f}^+ - \boldsymbol{f}^-)\nabla_x c_{\mathrm{b}}^0 + \nabla_y(\boldsymbol{f}^+ + \boldsymbol{f}^-)c_{\mathrm{b}}^0\nabla_x\overline{\psi}^0.$$

Using the above results the fluctuating part of the two latter terms of the r.h.s. of (29) can be represented as

$$\begin{aligned}2RT\Big[\big(\cosh\overline{\varphi}^0 - 1\big)\nabla_y c_{\mathrm{b}}^1 - \sinh\overline{\varphi}^0 c_{\mathrm{b}}^0\nabla_y\overline{\psi}^1\Big] &= RT\big[\big(\cosh\overline{\varphi}^0 - 1\big)\nabla_y(\boldsymbol{f}^+ + \boldsymbol{f}^-) - \sinh\overline{\varphi}^0\nabla_y(\boldsymbol{f}^+ - \boldsymbol{f}^-)\nabla_x c_{\mathrm{b}}^0\big]\\ &\quad + RT\Big[\big(\cosh\overline{\varphi}^0 - 1\big)\nabla_y(\boldsymbol{f}^+ - \boldsymbol{f}^-) - \sinh\nabla_y(\boldsymbol{f}^+ + \boldsymbol{f}^-)c_{\mathrm{b}}^0\nabla_x\overline{\psi}^0\Big]\end{aligned}$$

which give

$$\mu_{\mathrm{f}}\triangle_{yy}\mathbf{v}^0 - \nabla_y p_{\mathrm{b}}^1 = \nabla_x p_{\mathrm{b}}^0 + \boldsymbol{F}\nabla_x c_{\mathrm{b}}^0 + \boldsymbol{G}\nabla_x\overline{\psi}^0$$

with

$$\boldsymbol{F} = RT\big[2\big(\cosh\overline{\varphi}^0 - 1\big)\boldsymbol{I} + \big(\exp(-\overline{\varphi}^0) - 1\big)\nabla_y\boldsymbol{f}^+ + \big(\exp(+\overline{\varphi}^0) - 1\big)\nabla_y\boldsymbol{f}^-\big], \tag{55}$$

$$\boldsymbol{G} = RTc_{\mathrm{b}}^0\big[-2\sinh\overline{\varphi}^0\boldsymbol{I} + \big(\exp(-\overline{\varphi}^0) - 1\big)\nabla_y\boldsymbol{f}^+ - \big(\exp(+\overline{\varphi}^0) - 1\big)\nabla_y\boldsymbol{f}^-\big]. \tag{56}$$

The r.h.s. of the above result shows that in addition to a bulk phase pressure gradient flow is also driven by gradients in concentration (chemico-osmotic effect) and streaming potential (electro-osmotic effect). To derive Darcy's law we decompose the velocity and pressure fluctuation into their hydraulic, chemico-osmotic and electro-osmotic components $\mathbf{v}^0 = \mathbf{v}_p^0 + \mathbf{v}_c^0 + \mathbf{v}_e^0$ and $p_{\mathrm{b}}^1 = p_p^1 + p_c^1 + p_e^1$. The pair $\{\mathbf{v}_p^0, p_p^1\}$ satisfies the local Stokes problem only driven by pressure gradient

$$\begin{aligned}&\mu_{\mathrm{f}}\triangle_{yy}\mathbf{v}_p^0 - \nabla_y p_p^1 = \nabla_x p_{\mathrm{b}}^0,\\ &\nabla_y\cdot\mathbf{v}_p^0 = 0 \quad \text{in } Y_{\mathrm{f}},\\ &\mathbf{v}_p^0 = \tfrac{\partial\boldsymbol{u}^0}{\partial t} \quad \text{on } \partial Y_{\mathrm{fs}},\end{aligned}$$

whereas the chemico- and electro-osmotic components satisfy

$$\left.\begin{aligned}&\mu_{\mathrm{f}}\triangle_{yy}\mathbf{v}_c^0 - \nabla_y p_c^1 = \boldsymbol{F}\nabla_x c_{\mathrm{b}}^0,\\ &\nabla_y\cdot\mathbf{v}_c^0 = 0 \quad \text{in } Y_{\mathrm{f}},\\ &\mathbf{v}_c^0 = 0 \quad \text{on } \partial Y_{\mathrm{fs}},\end{aligned}\right| \left.\begin{aligned}&\mu_{\mathrm{f}}\triangle_{yy}\mathbf{v}_e^0 - \nabla_y p_e^1 = \boldsymbol{G}\nabla_x\overline{\psi}^0,\\ &\nabla_y\cdot\mathbf{v}_e^0 = 0 \quad \text{in } Y_{\mathrm{f}},\\ &\mathbf{v}_e^0 = 0 \quad \text{on } \partial Y_{\mathrm{fs}}.\end{aligned}\right.$$

Denoting $\{\boldsymbol{e}_j\}$, $(j = 1,2,3)$ an orthonormal basis, define the set of periodic characteristic tensorial functions $\{\boldsymbol{\kappa}_p, \boldsymbol{\kappa}_c, \boldsymbol{\kappa}_e\}$, with vectorial components $\{\boldsymbol{\kappa}_p^j, \boldsymbol{\kappa}_c^j, \boldsymbol{\kappa}_e^j\}$, $(j = 1,2,3)$ and the scalars $\{\widetilde{p}_p{}^1, \widetilde{p}_c{}^1, \widetilde{p}_e{}^1\}$ satisfying the following canonical problems

$$\begin{aligned}&\mu_{\mathrm{f}}\triangle_{yy}\boldsymbol{\kappa}_p^j - \nabla_y\widetilde{p}_p{}^1 = -\boldsymbol{e}_j,\\ &\nabla_y\cdot\boldsymbol{\kappa}_p^j = 0, \quad j = 1,2,3,\\ &\boldsymbol{\kappa}_p^j = 0 \quad \text{on } \partial Y_{\mathrm{fs}}\end{aligned}$$

and

$$\left.\begin{aligned}&\mu_{\mathrm{f}}\triangle_{yy}\boldsymbol{\kappa}_c^j - \nabla_y\widetilde{p}_c{}^1 = -\boldsymbol{F}\boldsymbol{e}_j\\ &\nabla_y\cdot\boldsymbol{\kappa}_c^j = 0,\\ &\boldsymbol{\kappa}_c^j = 0 \quad \text{on } \partial Y_{\mathrm{fs}},\end{aligned}\right| \left.\begin{aligned}&\mu_{\mathrm{f}}\triangle_{yy}\boldsymbol{\kappa}_e^j - \nabla_y\widetilde{p}_e{}^1 = -\boldsymbol{G}\boldsymbol{e}_j,\\ &\nabla_y\cdot\boldsymbol{\kappa}_e^j = 0, \quad j = 1,2,3,\\ &\boldsymbol{\kappa}_e^j = 0 \quad \text{on } \partial Y_{\mathrm{fs}}.\end{aligned}\right. \tag{57}$$

Hence, exploiting the linearity between the above results we obtain after averaging

$$\begin{aligned}
&\left\langle \mathbf{v}_p^0 - \frac{\partial \boldsymbol{u}^0}{\partial t} \right\rangle = -\boldsymbol{K}_P \nabla_x p_{\mathrm{b}}^0 \quad \text{with } \boldsymbol{K}_P \equiv \langle \boldsymbol{\kappa}_p \rangle, \\
&\langle \mathbf{v}_c^0 \rangle = -\boldsymbol{K}_C \nabla_x c_{\mathrm{b}}^0 \quad \text{with } \boldsymbol{K}_C \equiv \langle \boldsymbol{\kappa}_c \rangle, \\
&\langle \mathbf{v}_e^0 \rangle = -\boldsymbol{K}_E \nabla_x \overline{\psi}^0 \quad \text{with } \boldsymbol{K}_E \equiv \langle \boldsymbol{\kappa}_e \rangle.
\end{aligned} \tag{58}$$

Defining the Darcian velocity $\mathbf{v}_{\mathrm{D}}^0 \equiv \langle \mathbf{v}_{\mathrm{f}}^0 - \partial \boldsymbol{u}^0/\partial t \rangle + \langle \mathbf{v}_c^0 \rangle + \langle \mathbf{v}_e^0 \rangle$, Darcy's law is finally written

$$\mathbf{v}_{\mathrm{D}}^0 = -\boldsymbol{K}_P \nabla_x p_{\mathrm{b}}^0 - \boldsymbol{K}_C \nabla_x c_{\mathrm{b}}^0 - \boldsymbol{K}_E \nabla_x \overline{\psi}^0. \tag{59}$$

The above result resembles in form Darcy's law derived in Gu et al. (1998a). The first term in the r.h.s. quantifies flow driven by the bulk phase pressure gradient. This component has been termed the mechanochemical force, as it incorporates the difference between hydraulic and chemico-osmotic pressures $\nabla(p^0 - \pi^0)$. The middle term is the chemico-osmotic (gradient of the Nernst potential) and is particularly pronounced when the salinity varies spatially. The last term in the r.h.s. incorporates the electro-osmotic component which dictates flow driven by streaming potential gradients. The mechano-electrochemical coupling coefficients are defined thermodynamically in Gu et al. (1998a) in the spirit of Onsager's reciprocity relations. In the proposed formulation they arise naturally and can be computed precisely through their micromechanical representations (57) and (58). These representations provide important insight in the mechanisms that drive flow and in the physics underlying the coupling coefficients $\boldsymbol{K}_C$ and $\boldsymbol{K}_E$. In particular one may note that the functions $\boldsymbol{F}$ and $\boldsymbol{G}$ are governed by a leading component (first term in the r.h.s. of (55) and (56)) which is mainly related to the distribution of the electric potential across the pore space. In addition, one may observe that the fluctuations in the ions concentration (terms related to $\boldsymbol{f}^{\pm}$) also influence the magnitude of the coupling coefficients. For the particular case where the geometry of cell is composed of two parallel particles (stratified arrangement), since pressure and concentration are constant in each cross section, their fluctuations in the transversal direction vanish and thus the behavior of $\{\boldsymbol{F}, \boldsymbol{G}\}$ is only dictated by the variability of $\overline{\varphi}^0$ in the transversal direction. This reproduces the results of Sasidhar and Ruckenstein (1981) for the case of a stratified arrangement. The additional terms involving the fluctuations $\boldsymbol{f}^{\pm}$ in (55) and (56) aim at incorporating the local variability in the concentrations which arises when dealing with non-stratified arrangements. Further, if the thickness of the e.d.l. is small compared to the interlayer spacing, the first term in the r.h.s. of (57) for $\boldsymbol{G}$ leads to the well known Smoluchowski model (see e.g. Shang, 1997; Hunter, 1981; Coelho et al., 1996) which relates electro-osmotic permeability with the zeta potential (see Appendix A.2, Eq. (A.7) for details). Concerning the coupling mechanisms that drive fluid flow it should be noted that, as the streaming potential slows down the movement of the fluid and the ions to conserve charge (see Appendix A.4) the terms involving ∇c_{b}^0 and $\nabla \overline{\psi}^0$ act in opposite directions therefore competing with each other. In fact the electro-osmotic component $-\boldsymbol{K}_E \nabla \overline{\psi}^0$ leads to fluid movement toward the regions of higher concentration where the streaming potential is lower (see details in Appendix A.4, Eq. (A.9)) and therefore it plays the role of a true osmotic term. On the other hand, the chemico-osmotic component related to $-\boldsymbol{K}_C \nabla c_{\mathrm{b}}^0$ arises from the gradient of the osmotic pressure in analogy to the case of non-ionic solutions (see e.g. Barbour and Fredlund, 1989). The peculiar phenomena of anomalous (reverse) osmosis (discussed in e.g. GU et al. (1998b)) occurs when the chemico-osmotic component dominates the electro-osmotic one for a constant bulk phase pressure. When the frictions due to the electro-chemo effects (which are related to the inverse of the couplings coefficients $\boldsymbol{K}_C$ and $\boldsymbol{K}_E$) are of the same magnitude of the viscous friction (inverse of the hydraulic conductivity $\boldsymbol{K}_P$), Eq. (59) resembles in form the one postulated by Huyghe and Janssen (1997). In this case both $\boldsymbol{K}_C$ and $\boldsymbol{K}_E \approx \boldsymbol{K}_P$ and therefore the movement of te electrolyte solution is described by only one conductivity coefficient. Further, it should be noted that for particular microstructural morphologies where the condition $\nabla_x \cdot \boldsymbol{J}^0 = 0$ may be replaced by $\boldsymbol{J}^0 = 0$ (typically the one-

dimensional stratified microstructure of Appendix A), from (53) the electro-osmotic term can be eliminated in terms of the concentration gradient. This leads to the form (A.11) of Darcy's law, which resembles the one postulated in Barbour and Fredlund (1989) and Kaczmarek and Hueckel (1998), not including the term related to the streaming potential gradient.

4.2.5. Modified Terzaghi's decomposition

To derive the modified Terzaghi's effective principle we average the fluid and solid momentum balances (26)(a) and (40)(a). Using the divergence theorem, boundary condition (42)(b) and the periodicity we obtain the overall momentum balance

$$\nabla_x \cdot \boldsymbol{\sigma}_T^0 = 0, \quad \text{where } \boldsymbol{\sigma}_T^0 \equiv \begin{cases} \langle \boldsymbol{\sigma}_{\mathrm{f}}^0 \rangle & \text{in } Y_{\mathrm{f}}, \\ \langle \boldsymbol{\sigma}_{\mathrm{s}}^0 \rangle & \text{in } Y_{\mathrm{s}} \end{cases} \tag{60}$$

is the overall stress tensor of the mixture. The modified Terzaghi's effective stress principle can be obtained by considering the homogenized constitutive laws for $\langle \boldsymbol{\sigma}_{\mathrm{f}}^0 \rangle$ and $\langle \boldsymbol{\sigma}_{\mathrm{s}}^0 \rangle$. To this end we make use of (16) and rephrase the Neumann problem (39)(b) and (43) for $\boldsymbol{u}^1$ as

$$\begin{aligned} &\nabla_y \cdot \left(\boldsymbol{c}_{\mathrm{s}} \mathscr{E}_y(\boldsymbol{u}^1)\right) = 0 \quad \text{in } Y_{\mathrm{s}}, \\ &-\left[p_{\mathrm{b}}^0(\boldsymbol{x},t)\boldsymbol{I} + \boldsymbol{\Pi}_d^0(\boldsymbol{x},\boldsymbol{y},t)\right]\boldsymbol{n} = \boldsymbol{c}_{\mathrm{s}}\left[\mathscr{E}_x(\boldsymbol{u}^0(\boldsymbol{x},t)) + \mathscr{E}_y(\boldsymbol{u}^1)\right]\boldsymbol{n} \quad \text{on } \partial Y_{\mathrm{fs}}, \end{aligned} \tag{61}$$

where $\boldsymbol{\Pi}_d^0$ is a disjoining stress tensor which incorporates the chemico-osmotic pressure π^0 and Maxwell stresses $\boldsymbol{\tau}_{\mathrm{M}}^0$

$$\boldsymbol{\Pi}_d^0 = \pi^0 \boldsymbol{I} - \boldsymbol{\tau}_{\mathrm{M}}^0 = 2RTc_{\mathrm{b}}^0(\cosh \overline{\varphi}^0 - 1)\boldsymbol{I} - \boldsymbol{\tau}_{\mathrm{M}}^0. \tag{62}$$

When comparing the cell problem (61) for $\boldsymbol{u}^1$ with the similar Neumann problems arising in the homogenization derivation of Biot's equations of poroelasticity (see e.g. Terada et al., 1998; Auriault and Sanchez-Palencia, 1977; Auriault, 1990), the novelty is the appearance of the tensor $\boldsymbol{\Pi}_d^0$ which incorporates the influence of physico-chemical effects on the traction boundary condition. Eqs. (61) and (62) provide relevant information on the local stress analysis of charged particles. In particular, the one-dimensional scalar version of (62) for $\boldsymbol{\Pi}_d^0$ resembles in form the constitutive equations proposed for the electrostatic component of the disjoining pressure of plane-parallel thin liquid films (Derjaguin et al., 1987; Dahnert and Huster, 1999). By linearity we have

$$\boldsymbol{u}^1(\boldsymbol{x},\boldsymbol{y},t) = \boldsymbol{\zeta}(\boldsymbol{y})p_{\mathrm{b}}^0(\boldsymbol{x},t) + \boldsymbol{\xi}(\boldsymbol{y})\mathscr{E}_x(\boldsymbol{u}^0(\boldsymbol{x},t)) + \boldsymbol{u}_\pi^1(\boldsymbol{x},\boldsymbol{y},t) + \hat{\boldsymbol{u}}(\boldsymbol{x},t). \tag{63}$$

The canonical cell problems for the third-order tensor $\boldsymbol{\xi}$ and the vector $\boldsymbol{\zeta}$ are classical (Auriault, 1990; Terada et al., 1998; Lydzba and Shao, 2000).

$$\begin{aligned} &\nabla_y \cdot \left(\boldsymbol{c}_{\mathrm{s}} \mathscr{E}_y(\boldsymbol{\xi})\right) = 0 \quad \text{in } Y_{\mathrm{s}}, \ \left(\boldsymbol{c}_{\mathrm{s}} \mathscr{E}_y(\boldsymbol{\xi})\right)\boldsymbol{n} = -\boldsymbol{c}_{\mathrm{s}}\boldsymbol{I}\boldsymbol{I}\boldsymbol{n} \quad \text{on } \partial Y_{\mathrm{fs}}, \\ &\nabla_y \cdot \left(\boldsymbol{c}_{\mathrm{s}} \mathscr{E}_y(\boldsymbol{\zeta})\right) = 0 \quad \text{in } Y_{\mathrm{s}}, \ \left(\boldsymbol{c}_{\mathrm{s}} \mathscr{E}_y(\boldsymbol{\zeta})\right)\boldsymbol{n} = -\boldsymbol{I}\boldsymbol{n} \quad \text{on } \partial Y_{\mathrm{fs}}, \end{aligned} \tag{64}$$

where $\boldsymbol{I}\boldsymbol{I}$ denotes the unity fourth-order tensor. The novelty in (63) is the appearance of $\boldsymbol{u}_\pi^1$ which corresponds to the particle displacement component arising from the traction induced by the physico-chemical tensor $\boldsymbol{\Pi}_d^0$

$$\begin{aligned} &\nabla_y \cdot \left(\boldsymbol{c}_{\mathrm{s}} \mathscr{E}_y(\boldsymbol{u}_\pi^1)\right) = 0 \quad \text{in } Y_{\mathrm{s}}, \\ &\left(\boldsymbol{c}_{\mathrm{s}} \mathscr{E}_y(\boldsymbol{u}_\pi^1)\right)\boldsymbol{n} = -\boldsymbol{\Pi}_d^0\boldsymbol{n} \quad \text{on } \partial Y_{\mathrm{fs}}. \end{aligned} \tag{65}$$

Denoting $\boldsymbol{C}_{\mathrm{s}} \equiv \langle \boldsymbol{c}_{\mathrm{s}}(\boldsymbol{I}\boldsymbol{I} + \mathscr{E}_y(\boldsymbol{\xi}))\rangle$ the macroscopic elastic modulus (fourth-rank tensor) by averaging the constitutive equation (40)(b) for $\boldsymbol{\sigma}_{\mathrm{s}}^0$ and using (63) we obtain

$$\langle \boldsymbol{\sigma}_{\mathrm{s}}^0 \rangle = \boldsymbol{c}_{\mathrm{s}} \mathscr{E}_x(\boldsymbol{u}^0) + \langle \boldsymbol{c}_{\mathrm{s}} \mathscr{E}_y(\boldsymbol{\zeta})\rangle p_{\mathrm{b}}^0 + \langle \boldsymbol{c}_{\mathrm{s}} \mathscr{E}_y(\boldsymbol{u}_\pi^1)\rangle. \tag{66}$$

By rewriting the constitutive equation for $\boldsymbol{\sigma}_{\mathrm{f}}^0$ (27) in terms of p_{b}^0, using (16) and (62) we get after averaging $\langle\boldsymbol{\sigma}_{\mathrm{f}}^0\rangle = -n_{\mathrm{f}}p_{\mathrm{b}}^0\boldsymbol{I} - \langle\boldsymbol{\Pi}_d^0\rangle$. Using this result in definition (60) along with (66) we obtain

$$\boldsymbol{\sigma}_T^0 = -\boldsymbol{\alpha}p_{\mathrm{b}}^0 + \boldsymbol{C}_{\mathrm{s}}\mathscr{E}_x(\boldsymbol{u}^0) - \boldsymbol{\Pi}^0, \tag{67}$$

where $\boldsymbol{\alpha} \equiv n_{\mathrm{f}}\boldsymbol{I} - \langle\boldsymbol{c}_{\mathrm{s}}\mathscr{E}_y(\boldsymbol{\zeta})\rangle$ is the Biot coefficient for the particles and

$$\boldsymbol{\Pi}^0 = \langle\boldsymbol{\Pi}_d^0\rangle + n_{\mathrm{s}}\boldsymbol{\Pi}_S^0 \quad \text{with } \boldsymbol{\Pi}_S^0 \equiv -\langle\boldsymbol{c}_{\mathrm{s}}\mathscr{E}_y(\boldsymbol{u}_\pi^1)\rangle^s, \tag{68}$$

where $n_{\mathrm{s}} = 1 - n_{\mathrm{f}}$ is the volume fraction of the solid (recall that $\langle\cdot\rangle = n_{\mathrm{s}}\langle\cdot\rangle^s$). Eq. (67) is the macroscopic form of Terzaghi's decomposition for the compacted swelling clay. In addition to the pore pressure p_{b}^0 and contact stresses $\boldsymbol{C}_s\mathscr{E}_x(\boldsymbol{u}^0)$, it includes the macroscopic physico-chemical tensor $\boldsymbol{\Pi}^0$ which incorporates the influence of physico-chemical effects upon the overall stresses of the clay clusters $\boldsymbol{\sigma}_T^0$. From (68) this quantity may be decomposed into the averaged counterpart of $\boldsymbol{\Pi}_d^0$ (which from (62) is the sum of chemico-osmotic and Maxwell stresses) and the additional component $\boldsymbol{\Pi}_S^0$, which consists of chemical stresses in the particles due to the traction induced by $\boldsymbol{\Pi}_d^0$ in (65). Since $\boldsymbol{\Pi}_S^0$ represents stresses acting effectively in the solid phase, it may be viewed as the physico-chemical component directly responsible for the expansion of the aggregates. Whence, thus quantity shall be referred to as *swelling stress tensor* as it plays the role of a tensorial generalization of the swelling pressure to incorporate deviatoric effects. This alternative way of expressing the modified Terzaghi's principle resembles in form some heuristic modified effective stress principles for clays (see e.g. Sridharan and Rao, 1973 or Lambe, 1960). Historically, physico-chemical forces have heuristically been modeled at the macroscale through the addition of a term to Terzaghi's principle which measures the effect of net repulsive ($R\boldsymbol{I}$) and attractive ($A\boldsymbol{I}$) forces between particles. This stress is commonly denoted by $(R-A)\boldsymbol{I}$ (see Sridharan and Rao, 1973). In Lambe (1960)), effective stresses are defined as the difference between total stress and pore pressure whereas in Sridharan and Rao (1973) effective stresses are nothing but the matrix contact stresses (see Hueckel, 1992a). It should be noted that our macroscopic modified Terzaghi's effective stress principle (67) is capable of reproducing both Sridharan and Rao and Lambe's parallel connection models. The former can be recovered by simply defining effective stress as the contact elastic component $\boldsymbol{C}_{\mathrm{s}}\mathscr{E}_x(\boldsymbol{u}^0)$ whereas the latter as $\boldsymbol{C}_{\mathrm{s}}\mathscr{E}_x(\boldsymbol{u}^0) - \boldsymbol{\Pi}$. Thus,(67) is a first rational attempt at a rigorous micromechanical derivation of the above heuristic modified Terzaghi's principle in the case where $A = 0$.

In the case of stratified arrangements, an alternative description of the decomposition (68) can be adopted where the scalar versions of $\boldsymbol{\Pi}_d^0$ and $\boldsymbol{\Pi}_S^0$ can be precisely identified with Derjaguin's microscopic disjoining pressure (Derjaguin et al., 1987) and Low's macroscopic swelling pressure (Low, 1987) (see Appendix A.5).

4.2.6. Overall mass balance

Finally we derive the overall macroscopic mass balance. By averaging (24), using boundary condition (41)(c) together with the closure equation (63) and the divergence theorem we get

$$\begin{aligned}\langle\boldsymbol{\nabla}_x\cdot\mathbf{v}^0\rangle &= -\langle\boldsymbol{\nabla}_y\mathbf{v}^1\rangle = -\frac{1}{|Y|}\int_\Gamma \mathbf{v}^1\cdot\boldsymbol{n}\,\mathrm{d}\Gamma = -\frac{1}{|Y|}\int_\Gamma \frac{\partial\boldsymbol{u}^1}{\partial t}\cdot\boldsymbol{n}\,\mathrm{d}\Gamma\\ &= \left\langle\boldsymbol{\nabla}_y\cdot\frac{\partial\boldsymbol{u}^1}{\partial t}\right\rangle = \langle\boldsymbol{\nabla}_y\cdot\boldsymbol{\xi}\rangle : \frac{\partial}{\partial t}\mathscr{E}_x(\boldsymbol{u}^0) + \langle\boldsymbol{\nabla}_y\cdot\boldsymbol{\zeta}\rangle\frac{\partial p_{\mathrm{b}}^0}{\partial t} + \left\langle\boldsymbol{\nabla}_y\cdot\frac{\partial\boldsymbol{u}_\pi^1}{\partial t}\right\rangle,\end{aligned}$$

where $\boldsymbol{A}:\boldsymbol{B} = \mathrm{tr}(\boldsymbol{A}\boldsymbol{B}^{\mathrm{T}})$ denotes the classical inner product between tensors. By rewriting the above result in terms of the Darcian velocity $\mathbf{v}_{\mathrm{D}}^0$ we obtain

$$\boldsymbol{\nabla}_x\cdot\mathbf{v}_{\mathrm{D}}^0 + \boldsymbol{\alpha}^* : \frac{\partial}{\partial t}\mathscr{E}_x(\boldsymbol{u}^0) = \langle\boldsymbol{\nabla}_y\cdot\boldsymbol{\zeta}\rangle\frac{\partial p_{\mathrm{b}}^0}{\partial t} + \left\langle\boldsymbol{\nabla}_y\cdot\frac{\partial\boldsymbol{u}_\pi^1}{\partial t}\right\rangle, \tag{69}$$

where $\boldsymbol{\alpha}^* = n_f \boldsymbol{I} - \langle \nabla_y \cdot \boldsymbol{\xi} \rangle$. Further, by pursuing the analysis presented in Auriault and Sanchez-Palencia (1977) one can show the classical relation $\boldsymbol{\alpha}^* = n_f \boldsymbol{I} - \langle \boldsymbol{c}_s \mathscr{E}_y(\boldsymbol{\zeta}) \rangle = \boldsymbol{\alpha}$ commonly adopted in Biot's theory of poroelasticity. Finally, one may note the appearance of the additional last term in the r.h.s. of (69) which is related to the compressibility of the solid phase due the forces induced by the disjoining stress $\boldsymbol{\Pi}_d^0$.

4.2.7. Mass balance of the fluid phase

To close the system it remains to derive a mass balance for the fluid phase which shall be used to compute the porosity n_f. To this end we make use of the classical Reynolds transport theorem applied to a general scalar function f defined on Y_f. Denoting $\partial \boldsymbol{u}/\partial t$ the interfacial velocity and using the no-slip condition (10) we have

$$\frac{\partial \langle f \rangle}{\partial t} - \left\langle \frac{\partial f}{\partial t} \right\rangle = \frac{1}{|Y|} \int_{\partial Y_{fs}} f \frac{\partial \boldsymbol{u}}{\partial t} \cdot \boldsymbol{n} \, \mathrm{d}\Gamma = \frac{1}{|Y|} \int_{\partial Y_{fs}} f \mathbf{v} \cdot \boldsymbol{n} \, \mathrm{d}\Gamma$$

which for $f = 1$ gives

$$\frac{\partial n_f}{\partial t} = \frac{1}{|Y|} \int_{\partial Y_{fs}} \mathbf{v} \cdot \boldsymbol{n} \, \mathrm{d}\Gamma.$$

Further, using the spatial averaging theorem (Whitaker, 1999) for the mass balance of the incompressible fluid phase (2) yields

$$\langle \nabla \cdot \mathbf{v} \rangle = \nabla \cdot \langle \mathbf{v} \rangle + \frac{1}{|Y|} \int_{\partial Y_{fs}} \mathbf{v} \cdot \boldsymbol{n} \, \mathrm{d}\Gamma = 0.$$

Combining the above results we get

$$\frac{\partial n_f}{\partial t} + \nabla \cdot \langle \mathbf{v} \rangle = 0.$$

Using the asymptotic developments the above relation can be written as

$$\frac{\partial n_f}{\partial t} + \left(\nabla_x + \epsilon^{-1} \nabla_y \right) \cdot \left(\langle \mathbf{v}^0 \rangle + \epsilon \langle \mathbf{v}^1 \rangle \right) = \mathscr{O}(\epsilon).$$

Hence, recalling that averaged properties are independent of $\boldsymbol{y}$ we obtain at $\mathscr{O}(1)$

$$\frac{\partial n_f}{\partial t} + \nabla_x \cdot \langle \mathbf{v}^0 \rangle = 0.$$

Finally, by rewriting the above result in terms of the Darcy velocity $\mathbf{v}_D^0 = \langle \mathbf{v}^0 - \partial \boldsymbol{u}^0/\partial t \rangle$ and neglecting the convective effects induced by $\partial \boldsymbol{u}^0(\boldsymbol{x}, t)/\partial t$ we obtain

$$\frac{\partial n_f}{\partial t} + \nabla_x \cdot \mathbf{v}_D^0 + n_f \nabla_x \cdot \frac{\partial \boldsymbol{u}^0}{\partial t} = 0.$$

4.3. Summary of the two-scale model

Denote $\{\boldsymbol{\zeta}, \boldsymbol{\xi}, \boldsymbol{\kappa}_p\}$ and $\{\boldsymbol{\kappa}_c, \boldsymbol{\kappa}_e, \boldsymbol{f}^+, \boldsymbol{f}^-\}$ sets of the aforementioned characteristic functions with the former set depending on cell geometry and the latter also depending on the salt concentrations $c_b^0(\boldsymbol{x}, t)$. The two-scale model consists in finding the macroscopic variables $\{\boldsymbol{\sigma}_T^0, \boldsymbol{u}^0, p_b^0, \mathbf{v}_D^0, c_b^0, \psi^0, n_f\}$ satisfying

$$\begin{cases} \nabla_x \cdot \boldsymbol{\sigma}_T^0 = 0, \\ \boldsymbol{\sigma}_T^0 = -\boldsymbol{\alpha} p_{\mathrm{b}}^0 + \boldsymbol{C}_{\mathrm{s}} \mathscr{E}_x(\boldsymbol{u}^0) - \boldsymbol{\Pi}^0, \\ \mathbf{v}_{\mathrm{D}}^0 = -\boldsymbol{K}_P \nabla_x p_{\mathrm{b}}^0 - \boldsymbol{K}_C \nabla_x c_{\mathrm{b}}^0 - \boldsymbol{K}_E \nabla_x \overline{\psi}^0, \\ \nabla_x \cdot \mathbf{v}_{\mathrm{D}}^0 + \boldsymbol{\alpha} : \dfrac{\partial}{\partial t} \mathscr{E}_x(\boldsymbol{u}^0) = \beta \dfrac{\partial p_{\mathrm{b}}^0}{\partial t} + \dfrac{\partial \gamma_\pi}{\partial t}, \\ \dfrac{\partial}{\partial t}\left(n_{\mathrm{f}} G_\varphi^{\pm} c_{\mathrm{b}}^0 \right) = \nabla_x \cdot \left[n_{\mathrm{f}} \boldsymbol{D}_{\pm}^* \left(\nabla_x c_{\mathrm{b}}^0 \pm c_{\mathrm{b}}^0 \nabla_x \overline{\psi}^0 \right) \right], \\ \dfrac{\partial n_{\mathrm{f}}}{\partial t} + \nabla_x \cdot \langle \mathbf{v}_{\mathrm{D}}^0 \rangle + n_{\mathrm{f}} \nabla_x \cdot \dfrac{\partial \boldsymbol{u}^0}{\partial t} = 0 \quad \text{in } \Omega, \end{cases} \tag{70}$$

where the component $\boldsymbol{\Pi}^0$ and the coefficients $\{\boldsymbol{\alpha}, \boldsymbol{C}_{\mathrm{s}}, \boldsymbol{K}_P, \boldsymbol{K}_C, \boldsymbol{K}_E, \beta, \gamma_\pi, \boldsymbol{D}_{\pm}^*, G_\varphi\}$ admit the micromechanical representations in the unit cell Y

$$\begin{aligned} &\boldsymbol{\Pi}^0 = \langle \pi^0 \boldsymbol{I} - \boldsymbol{\tau}_{\mathrm{M}}^0 \rangle + n_{\mathrm{s}} \boldsymbol{\Pi}_S^0, \qquad \pi^0 = 2RTc_{\mathrm{b}}^0(\cosh \overline{\varphi}^0 - 1)), \\ &\boldsymbol{\tau}_{\mathrm{M}}^0 = \frac{\tilde{\varepsilon}\tilde{\varepsilon}_0}{2}\left(2\boldsymbol{E}^0 \otimes \boldsymbol{E}^0 - (E^0)^2 \boldsymbol{I} \right), \qquad \boldsymbol{\Pi}_S^0 = -\langle \boldsymbol{c}_{\mathrm{s}} \mathscr{E}_y(\boldsymbol{u}_\pi^1) \rangle^s, \\ &\boldsymbol{\alpha} = n_{\mathrm{f}} \boldsymbol{I} - \langle \boldsymbol{c}_{\mathrm{s}} \mathscr{E}_y(\boldsymbol{\zeta}) \rangle = n_{\mathrm{f}} \boldsymbol{I} - \langle \nabla_y \cdot \boldsymbol{\xi} \rangle, \qquad \boldsymbol{C}_{\mathrm{s}} = \langle \boldsymbol{c}_{\mathrm{s}} (\boldsymbol{II} + \mathscr{E}_y(\boldsymbol{\xi})) \rangle, \\ &\boldsymbol{K}_P = \langle \boldsymbol{\kappa}_p \rangle, \quad \boldsymbol{K}_C = \langle \boldsymbol{\kappa}_c \rangle, \quad \boldsymbol{K}_E = \langle \boldsymbol{\kappa}_e \rangle, \quad \beta = \langle \nabla_y \cdot \boldsymbol{\zeta} \rangle, \\ &\frac{\partial \gamma_\pi}{\partial t} = \left\langle \nabla_y \cdot \frac{\partial \boldsymbol{u}_\pi^1}{\partial t} \right\rangle, \qquad \boldsymbol{D}_{\pm}^* = \langle \mathscr{D}_{\pm} \exp(\mp \overline{\varphi}^0)(\boldsymbol{I} + \nabla_y \boldsymbol{f}^{\pm}) \rangle^f, \\ &G_\varphi^{\pm} = \langle \exp(\mp \overline{\varphi}^0) \rangle^f \end{aligned} \tag{71}$$

with the set of local variables $\{\varphi^0, \boldsymbol{E}^0, \boldsymbol{u}_\pi^1\}$ satisfying the Neumann problems

$$\left.\begin{array}{l} \tilde{\varepsilon}\tilde{\varepsilon}_0 \triangle_{yy} \varphi^0 = 2Fc_{\mathrm{b}}^0 \sinh \overline{\varphi}^0, \\ \boldsymbol{E}^0 = -\nabla_y \varphi^0 \quad \text{in } Y_{\mathrm{f}}, \\ \tilde{\varepsilon}\tilde{\varepsilon}_0 \boldsymbol{E}^0 \cdot \boldsymbol{n} = -\sigma \quad \text{on } \partial Y_{\mathrm{fs}}, \end{array}\right| \left.\begin{array}{l} \nabla_y \cdot \left(\boldsymbol{c}_{\mathrm{s}} \mathscr{E}_y(\boldsymbol{u}_\pi^1) \right) = 0 \quad \text{in } Y_{\mathrm{s}}, \\ \left(\boldsymbol{c}_{\mathrm{s}} \mathscr{E}_y(\boldsymbol{u}_\pi^1) \right) \boldsymbol{n} = -(\pi^0 \boldsymbol{I} - \boldsymbol{\tau}_{\mathrm{M}}^0) \boldsymbol{n} \quad \text{on } \partial Y_{\mathrm{fs}}. \end{array}\right. \tag{72}$$

An essential feature of the above two-scale formulation is the communication between the macroscopic and microstructural behaviors of the swelling medium which appear naturally in the couplings between global and local unit cell problems. In this approach the information on the microstructural morphology of the swelling medium is incorporated in the two-scale model through the geometry of the unit periodic cell and the magnitude of the local parameters (such as e.g. the surface charge density σ). Different cell geometries lead to different solutions of the closure problems and therefore to different homogenized coefficients.

In what follows we shall consider a particular case of the two-scale model wherein the particles are isotropic and nearly incompressible with respect to the coupling problem (64)(b) for the coefficients $\boldsymbol{\alpha}$ and β such that $\boldsymbol{c}_{\mathrm{s}} \mathscr{E}_y(\boldsymbol{\zeta}) = -\boldsymbol{I}$ and $\nabla_y \cdot \boldsymbol{\zeta} = 0$. Hence we have $\langle \boldsymbol{c}_{\mathrm{s}} \mathscr{E}_y(\boldsymbol{\zeta}) \rangle = -n_{\mathrm{s}} \boldsymbol{I}$, $\boldsymbol{\alpha} = \boldsymbol{I}$ and $\beta = 0$ which implies that the overall mass balance reduces to $\nabla_x \cdot \mathbf{v}_{\mathrm{D}}^0 + (\partial \mathrm{div}\, \boldsymbol{u}^0 / \partial t) = 0$. This reproduces the classical Biot's poro-elasticity results where the coefficient β governs compressibility effects whereas α is ruled by the ratio between the bulk modulus of the solid and matrix (see e.g. Biot and Willis, 1957). Moreover, under the same nearly incompressibility assumption we also consider $\nabla_y \cdot \boldsymbol{u}_\pi^1 = \gamma_\pi = 0$.

The above system is supplemented by macroscopic initial and boundary conditions. Denoting $\Gamma = \Gamma_1 \cup \Gamma_2$, with Γ_1 and Γ_2 disjoint subsets of Γ and $\boldsymbol{N}$ the macroscopic unit outward normal, we consider the following set of boundary and initial conditions

$$\begin{aligned}
&\operatorname{div}_x \boldsymbol{u} = 0; \quad c_{\mathrm{b}}^0 = c_0 \quad \text{in } \Omega, \quad t = 0,\\
&\boldsymbol{\sigma N} = \boldsymbol{h}, \quad \mathbf{v}_{\mathrm{D}} \cdot \boldsymbol{N} = 0, \quad c_{\mathrm{b}}^0 = c_*; \quad \boldsymbol{J}^0 \cdot \boldsymbol{N} = 0 \quad \text{on } \Gamma_1,\\
&\boldsymbol{u} = 0, \quad p = 0; \quad \nabla_x c_{\mathrm{b}}^0 \cdot \boldsymbol{N} = \boldsymbol{J}^0 \cdot \boldsymbol{N} = 0 \quad \text{on } \Gamma_2,
\end{aligned} \tag{73}$$

where c_0 and c^* denote respectively prescribed concentrations and $\boldsymbol{h}$ denote a traction condition. The interface Γ_1 corresponds to a loaded mechanically impermeable base with prescribed concentration and electric current whereas Γ_2 corresponds to a rigid, permeable wall with free drainage, though impermeable to diffusive ion transport. Note that using the definition (53) for $\boldsymbol{J}^0$ implies $\nabla_x \overline{\psi}^0 \cdot \boldsymbol{N} = 0$ on Γ_2

5. Variational formulation and finite element approximation

We now turn to the approximation of the two-scale model by the finite element method. To this end we begin by considering the variational statement of the problem. Denote $L^2(\Omega)$ and $L^2(Y_i)(i = \mathrm{f}, \mathrm{s})$ the usual spaces of square integrable scalar valued functions equipped with the inner products

$$\begin{aligned}
&(f,g)_0 \equiv \int_\Omega fg \,\mathrm{d}\Omega \quad \forall f,g \in L^2(\Omega),\\
&(f,g)_1 \equiv \int_{Y_i} fg \,\mathrm{d}Y \quad \forall f,g \in L^2(Y_i), \quad i = \mathrm{f}, \mathrm{s}
\end{aligned}$$

and also let $H^1(\Omega) \times H^1(Y_i)$ be the usual subspaces of $L^2(\Omega) \times L^2(Y_i)$ given by

$$\begin{aligned}
&H^1(\Omega) \equiv \{f \in L^2(\Omega), \nabla f \in (L^2(\Omega))^3\},\\
&H^1(Y_i) \equiv \{f \in L^2(Y_i), \nabla f \in (L^2(Y_i))^3\}.
\end{aligned}$$

Considering the boundary conditions (73), introduce the appropriate function spaces for the macroscopic unknowns

$$\begin{aligned}
&\boldsymbol{U} \equiv \{\mathbf{v} \in (H^1(\Omega))^3, \quad \mathbf{v} = 0 \quad \text{on } \Gamma_2\},\\
&V \equiv \{q \in H^1(\Omega), \quad q = 0 \quad \text{on } \Gamma_2\},\\
&W^1 \equiv \{w \in H^1(\Omega), \quad w = c_* \quad \text{on } \Gamma_1\},\\
&W^2 \equiv \{w \in H^1(\Omega), \quad w = 0 \quad \text{on } \Gamma_1\}.
\end{aligned}$$

The variational formulation for the macroscopic problem (70) (with $\boldsymbol{\alpha} = \boldsymbol{I}$ and $\beta = \gamma_\pi = 0$) consists in: For each $t \in (0,\infty)$, find $\{\boldsymbol{u}^0(t), p_{\mathrm{b}}^0(t), c_{\mathrm{b}}^0(t), \psi^0(t)\} \in \boldsymbol{U} \times V \times W^1 \times H^1(\Omega)$ such that:

$$\begin{aligned}
&\left(\boldsymbol{C}_{\mathrm{s}} \mathscr{E}_x(\boldsymbol{u}^0), \mathscr{E}_x(\mathbf{v})\right)_0 - \left(p_{\mathrm{b}}^0, \operatorname{div}_x \mathbf{v}\right)_0 - \left(\boldsymbol{\Pi}^0, \mathscr{E}_x(\mathbf{v})\right)_0 = F^*(\mathbf{v}) \quad \forall \mathbf{v} \in \boldsymbol{U},\\
&\left(\operatorname{div}_x \frac{\partial \boldsymbol{u}^0}{\partial t}, q\right)_0 + \left(\boldsymbol{K}_P \nabla_x p_{\mathrm{b}}^0, \nabla_x q\right)_0 + \left(\boldsymbol{K}_C \nabla_x c_{\mathrm{b}}^0, \nabla_x q\right)_0 + \left(\boldsymbol{K}_E \nabla_x \overline{\psi}^0, \nabla_x q\right)_0 = 0 \quad \forall q \in V,\\
&\frac{\partial}{\partial t}\left(n_{\mathrm{f}} G_\varphi^{\pm} c_{\mathrm{b}}^0, w\right)_0 + \left(n_{\mathrm{f}} \boldsymbol{D}_\pm^* \left(\nabla_x c_{\mathrm{b}}^0 \pm c_{\mathrm{b}}^0 \nabla_x \overline{\psi}^0\right), \nabla_x w\right)_0 = 0 \quad \forall w \in W^2
\end{aligned} \tag{74}$$

with the reduced set of coefficients $\{\boldsymbol{c}_{\mathrm{s}}, \boldsymbol{K}_P, \boldsymbol{K}_C, \boldsymbol{K}_E, \boldsymbol{D}_\pm^*, \boldsymbol{\Pi}^0\}$ represented by the micromechanics in (71) and the porosity n_{f} and the linear functional $F^*(\mathbf{v})$ given by

$$\frac{\partial n_{\mathrm{f}}}{\partial t} = -\nabla_x \cdot \mathbf{v}_{\mathrm{D}}^0 - n_{\mathrm{f}} \nabla_x \cdot \frac{\partial \boldsymbol{u}^0}{\partial t}; \quad F^*(\mathbf{v}) = \int_{\Gamma_1} \boldsymbol{h} \cdot \mathbf{v} \,\mathrm{d}\Gamma. \tag{75}$$

In addition, the weak form of the local unit cell problems (72) for φ^0 and $\boldsymbol{u}_\pi^1$ can be stated as: For given $c_{\mathrm{b}}^0(\boldsymbol{x},t)$ and $\boldsymbol{\Pi}_d^0$ find $\{\varphi^0(t),\boldsymbol{u}_\pi^1(t)\}\in H^1(Y_{\mathrm{f}})\times(H^1(Y_{\mathrm{s}}))^3$ such that:

$$\tilde{\varepsilon}\tilde{\varepsilon}_0\left(\boldsymbol{\nabla}_y\varphi^0,\boldsymbol{\nabla}_y v\right)_1+2Fc_{\mathrm{b}}^0\left(\sinh\overline{\varphi}^0,v\right)_1=f(v)\quad\forall v\in H^1(Y_{\mathrm{f}}),\tag{76}$$

$$\left(\boldsymbol{c}_{\mathrm{s}}\mathscr{E}_y(\boldsymbol{u}_\pi^1),\mathscr{E}_y(\boldsymbol{\tau})\right)_1=g(\boldsymbol{\tau})\quad\forall\boldsymbol{\tau}\text{ in }(H^1(Y_{\mathrm{s}}))^3\tag{77}$$

with

$$f(v)=\int_{\partial Y_{\mathrm{fs}}}\sigma v\,\mathrm{d}\Gamma,\quad g(v)=-\int_{\partial Y_{\mathrm{fs}}}\boldsymbol{\Pi}_d^0\boldsymbol{n}\cdot\boldsymbol{\tau}\,\mathrm{d}\Gamma,\quad\boldsymbol{\Pi}_d^0=\pi^0\boldsymbol{I}-\boldsymbol{\tau}_{\mathrm{M}}^0.$$

5.1. Fully discrete backward Euler–Galerkin formulation

We now discuss the approximations in time and space of the above variational formulation. In what follows we discretize the macroscopic system (74) by the Galerkin method coupled with a time integration scheme. We consider a particular numerical example of a stratified clay whose microstructure is composed of long parallel particles. Moreover, we make use of the assumption of low electric potentials where the Poisson–Boltzmann is approximated by the Debye–Hueckel linearized form (see Appendix A, Eq. (A.1)). Under these assumptions the simplified form of the local cell problems (76) and (77) exhibit analytical solutions (see Appendix A for details). Consequently the discretization technique is applied to the macroscopic system whereas analytical solutions of the local cell problems are used to update the macroscopic parameters in (74) at each time. Thus, Let Δt be a fixed time step and denote $\{\boldsymbol{U}_h,V_h,W_h^1,W_h^2,X_h\}$ the families of finite dimensional subspaces of $\{\boldsymbol{U},V,W^1,W^2,H^1(\Omega)\}$ containing continuous, equal order piecewise polynomials on triangles or quadrilaterals of a partition of Ω of degree k. Denoting γ^m the approximation of a variable γ at $t_m=m\Delta t$, the backward Euler operator ∂_t approximates the time derivative by the quotient $\partial_t\gamma^m=(\gamma^m-\gamma^{m-1})\Delta t^{-1}$. The fully discrete scheme adopted herein is based on the classical backward Euler Galerkin method defined as: For each time $t=t_m=m\Delta t$ $(m\geqslant 1)$, find the macroscopic unknowns $\{\boldsymbol{u}_h^{0m},p_{bh}^{0m},c_{bh}^{0m},\psi_h^{0m}\}\in\boldsymbol{U}_h\times V_h\times W_h^1\times X_h$ satisfying

$$\left(\boldsymbol{C}_{\mathrm{s}}\mathscr{E}_x(\boldsymbol{u}_h^{0m}),\mathscr{E}_x(\mathbf{v}_h)\right)_0-\left(p_{bh}^{0m},\mathrm{div}_x\,\mathbf{v}_h\right)_0-\left(\boldsymbol{\Pi}^{0m},\mathscr{E}_x(\mathbf{v}_h)\right)_0=F^*(\mathbf{v}_h)\quad\forall\mathbf{v}_h\in\boldsymbol{U}_h,\tag{78}$$

$$\begin{aligned}\left(\mathrm{div}_x\,\boldsymbol{u}_h^{0m},q_h\right)_0+\Delta t\left(\boldsymbol{K}_P^m\boldsymbol{\nabla}_x p_{bh}^{0m},\boldsymbol{\nabla}_x q_h\right)_0&=-\Delta t\left(\boldsymbol{K}_C^m\boldsymbol{\nabla}_x c_{bh}^{0m},\boldsymbol{\nabla}_x q_h\right)_0-\Delta t\left(\boldsymbol{K}_E^m\boldsymbol{\nabla}_x\overline{\psi}_h^{0m},\boldsymbol{\nabla}_x q_h\right)_0\\&\quad+\left(\mathrm{div}_x\,\boldsymbol{u}_h^{0(m-1)},q_h\right)_0\quad\forall q_h\in V_h,\end{aligned}\tag{79}$$

$$\left(n_{\mathrm{f}}^m G_\varphi^{\pm m}c_{bh}^{0m},w_h\right)_0+\Delta t\left(n_{\mathrm{f}}^m\boldsymbol{D}_\pm^{*m}(\boldsymbol{\nabla}_x c_{bh}^{0m}\pm c_{bh}^{0m}\boldsymbol{\nabla}_x\overline{\psi}_h^{0m}),\boldsymbol{\nabla}_x w_h\right)_0=\left(n_{\mathrm{f}}^{m-1}G_\varphi^{\pm(m-1)}c_{bh}^{0(m-1)},w_h\right)_0\quad\forall w_h\in W_h^2,\tag{80}$$

where $\mathrm{div}\,\boldsymbol{u}_h^{00}=0$ and $c_{bh}^{00}=c_0$, In addition, at each time step, the linearized set of coefficients $\{\boldsymbol{\Pi}^{0m},\boldsymbol{K}_P^m,\boldsymbol{K}_C^m,\boldsymbol{K}_E^m,\boldsymbol{D}_\pm^{*m}\}$ are given analytically by the simplified micromechanical representations presented in Appendix A.

Due to the strong dependence of the macroscopic coefficients on the salinity c_{b}^0 and porosity n_{f} through the micromechanical representations, the aforementioned fully discrete formulation leads to a system of non-linear algebraic equations for the unknowns $\{\boldsymbol{u}_h^{0m},p_{bh}^{0m},c_{bh}^{0m},\overline{\psi}_h^{0m}\}$. For each time t_m the system is linearized using a Picard's relaxation type algorithm. After convergence is achieved for a given tolerance we proceed to the next time step. For each iteration, the resultant linear system is solved in a staggered fashion wherein (78) and (79) are first solved for $\{\boldsymbol{u}_h^{0m},p_h^{0m}\}$ with the r.h.s. evaluated at the previous iteration. Subsequently

the solution of the diffusion equations (80) for $\{c_{bh}^{0m}, \overline{\psi}_h^{0m}\}$ is computed with the coefficients calculated from the previous iteration.

6. Clay liner application

We consider an example concerning contaminant migration and electrokinetic attenuation through a compacted clay liner underneath a sanitary landfill. The problem consists of a geocomposite liner (described in the sense of Smith (1999)) composed of a volume of waste and a geomembrane overlying a compacted clay liner which lies immediately above a saturated aquifer (Fig. 1). The geomembrane corresponds to the top boundary Γ_1 representing an impermeable barrier to fluid flow, whereas the boundary Γ_2 represents a rigid and permeable interface between the liner and the aquifer. For simplicity we consider only chloride and sodium migration through the liner with a given bulk concentration of the leachate $c_b^0 = c_*$ on the top boundary Γ_1. In addition to the chemical aspects induced by the diffusion of Na^+ and Cl^- we also consider the settlement due to the load induced by the placement of the waste in the landfill Smith (1999) which is measured by the traction $\boldsymbol{h}$ in (73). Thus, the geomembrane transfers both chemical and mechanical consolidation from the upper boundary. For simplicity we assume that the contaminant is placed at the landfill at the same time of the beginning of the consolidation process. The bottom rigid interface Γ_2 between the liner and aquifer, though permeable to fluid flow, is considered a barrier for the diffusive transport of the leachates.

In Fig. 1 the origin of the longitudinal coordinate axis x is located at the top of the soil liner. Denoting L_0 the height of the liner, the boundaries Γ_1 and Γ_2 correspond to the locations $x = 0$ and $x = L_0$ respectively. In the idealized stratified microstructure the clay particles are oriented parallel to the longitudinal axis and therefore flow and transport take place only in the direction of the layers parallel to the x coordinate. Conversely, the disjoining stress tensor reduces to a scalar disjoining pressure Π_d^0 which acts in the normal

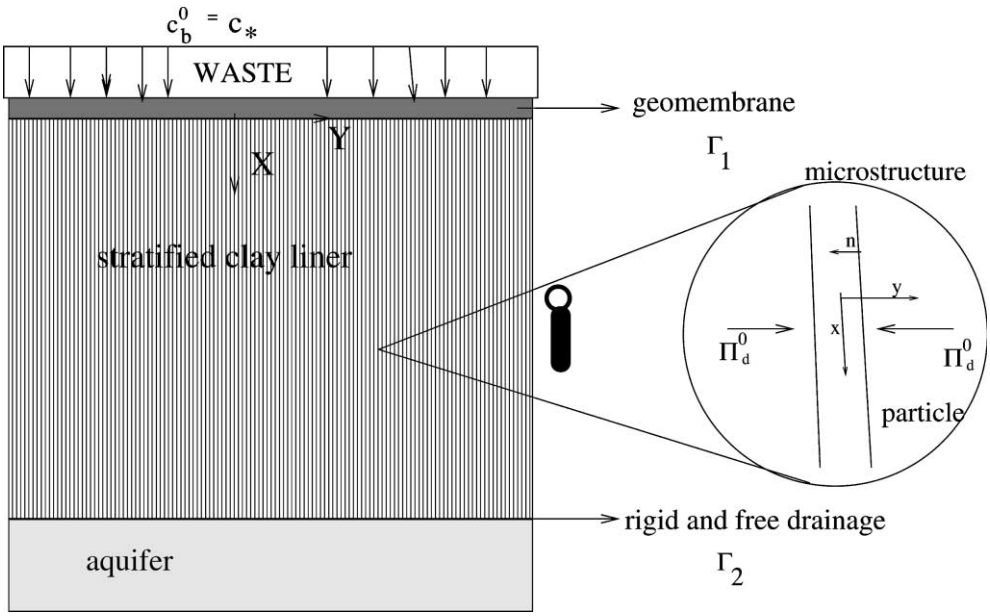

Fig. 1. Geocomposite liner and a zoom of the stratified microstructure composed of parallel particles.

(or transversal) direction parallel to the unitary vector $\boldsymbol{n}$ normal to the clay surface (Fig. 1). Further, in the particular case of stratified microstructure, one may use the arguments of the e.d.l. theory to show that Π_d^0 is constant in the interlayer spacing (see Appendix A.5, Eq. (A.15)). Hence, the one-dimensional solution of the unit cell problem (65) in the normal direction is $\boldsymbol{c}_s\mathscr{E}_y(\boldsymbol{u}_\pi^1) = -\Pi_d^0\boldsymbol{n}\otimes\boldsymbol{n}$ which shows an unique non-zero normal compression component equal to the disjoining pressure. By averaging this result and using definition (68)(b) we obtain $\boldsymbol{\Pi}_S^0 = \Pi_d^0\boldsymbol{n}\otimes\boldsymbol{n}$. Thus, defining the swelling pressure Π_S^0 as the projection $\Pi_S^0 \equiv \boldsymbol{\Pi}_S^0\boldsymbol{n}\cdot\boldsymbol{n}$ we then have $\Pi_S^0 = \Pi_d^0$. This result reproduces the classical Derjaguin's statement that for a parallel particle arrangement, the swelling pressure is nothing but the intrinsic averaging of the disjoining pressure (see Derjaguin et al., 1987).

A particular consequence of the one-dimensional stratified microstructure is that the macroscopic coefficients reduce to scalar quantities which dictate the behavior of the swelling medium in the axial direction. Conversely, the magnitude of these coefficients is strongly dependent on the e.d.l. and the solution of the linearized Poisson–Boltzmann problem in the transversal direction, normal to the clay surfaces. Thus, our numerical example is ruled by two different sets of macro/micro coefficients acting in orthogonal directions. In this configuration, the information provided by the microscopic e.d.l. is used to quantify the macroscopic parameters at each time. Due to the well known susceptibility of the diffuse double layer to change in the salinity c_b^0, as the concentration of the leachate evolves in time, particle separation decreases leading to a collapse of the fine pores and to a reduction in porosity. By considering a transversal fixed overburden load P_F, the swelling pressure is given as $\Pi_S^0 = \Pi_d^0 = P_F - p_b^0$. This result represents a simplified form of the momentum balance in the transversal direction (recall that since the particles are parallel, the transversal Terzaghi's stress component vanishes). After computing $\{\boldsymbol{u}_h^{0m}, p_{bh}^{0m}, c_{bh}^{0m}, \psi_h^{0m}\}$ at each Picard iteration this result can be applied in conjunction with the well known representation for Π_S^0 in the Debye–Hueckel approximation of the e.d.l. (Eq. (A.15)) leading to a relation which can be used to update the porosity n_f at each iteration. In the numerical results presented next, we consider that changes in the porosity n_f are mainly dictated by changes in the interlayer spacing H in the transversal direction. When combined with the mass balance (75) this also can be used to compute the transversal component of the displacement of the solid phase.

6.1. Numerical results

In what follows the subsequent numerical simulations aim at illustrating the potential of the two-scale approach in providing an accurate description of the decrease of the micro-porosity (due to the contraction of the e.d.l.) with the evolution of the brine concentration. The figures display the evolution of the dimensionless macroscopic quantities during the contaminant migration through the liner. The corresponding dimensionless quantities are denoted by the superscript "*" and are defined in Appendix B. Fig. 2 depicts the spatial variation of the dimensionless salinity $c_b^* = c_b^0/c_*$ with the axial coordinate $x^* = x/L_0$ for different times $t^* = (\lambda_s + 2\mu_s)K_{\text{Pref}}t/L_0^2$, where K_{Pref} is the value of K_P initially (see Appendix B). Since an increase in c_b^* (equal to one in the top of the liner at $x^* = 0$) leads to the suppression of the double layers, the locations of high concentration are associated with regions of low porosity as depicted in Fig. 3. As the concentration of the contaminant evolves in time the porosity at the bottom of the liner gradually decreases. The steady state configuration is characterized by a constant unitary concentration associated with an uniform low porosity. Also, note that as the velocity vanishes on the top of the liner due to the no-slip condition with the geomembrane, the pore pressure next to the geomembrane $p_b^0(x^* = 0, t = 0^+)$ decreases locally to give rise to a local sharp pressure gradient which opposes the abrupt concentration gradient at $t = 0$ in the one-dimensional form of Darcy's law (see Appendix A.2, Eq. (A.11)). Since $\Pi_d^0 = P_F - p_b^0$, this local boundary layer effect implies in an increase in the disjoining pressure close to $x = 0$ which also leads to an abrupt porosity drop at $t = 0$ even beyond its state value. As times evolves this sharp boundary layer effect dissipates and the porosity approaches the steady state value associated to the unitary concentration.

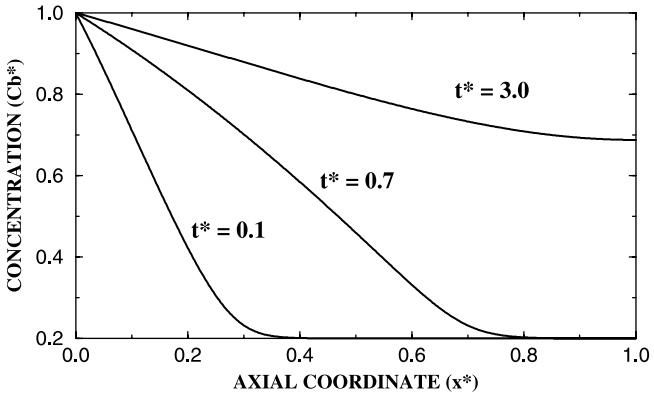

Fig. 2. Spatial distribution of the concentration for different times.

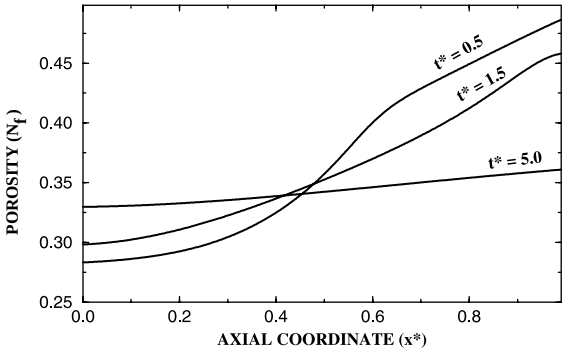

Fig. 3. Spatial distribution of the porosity for different times.

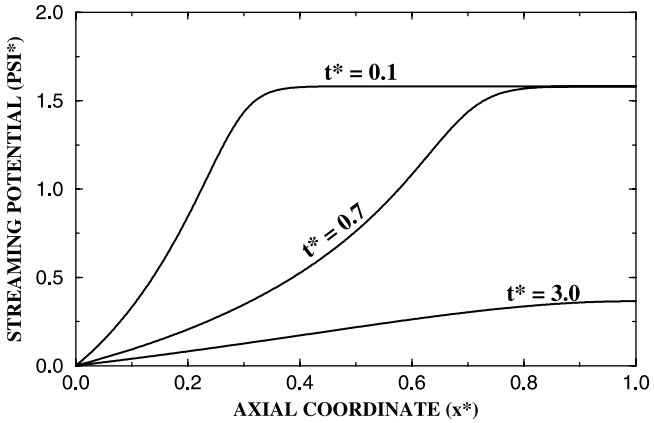

Fig. 4. Spatial distribution of the streaming potential for different times.

This stationary value of n_f is much lower compared to the initial one but slightly higher compared to the value $n_f^0(x = 0, t = 0^+)$ (see Fig. 3).

Fig. 4 depicts the spatial variation and time evolution of the dimensionless streaming potential $\overline{\psi}^0$, which is computed within a post-processing approach using (A.9). This quantity is calculated up to an additive constant which is arbitrarily set equal to zero at the top of the liner. As expected, its negative gradient is pointing upward which shows that electro-osmotic component slows down fluid flow and cation migration. As time evolves the gradient of the streaming potential decreases and vanishes at steady state.

7. Conclusion

We have presented an homogenization procedure for derivation of a macroscopic model for montmorillonite expansive clays. The model was derived by scaling up the pore-scale description which consists of the electro-hydrodynamics coupled with Nernst–Planck equations and the Poisson–Boltzmann problem which govern the fluid movement, ion transport and local electrostatics in the electrolyte solution. This led to a two-scale model where the macroscopic behavior appears somewhat related to the response of the microstructure. The essential feature underlying the micromechanical formulation proposed herein is the alternative way of representing the macroscopic parameters such as the swelling pressure and the electrokinetic coefficients which commonly appear in the framework of Onsager's reciprocity relations. This provides a new comprehensive understanding of the physics underlying electro-chemo-mechanical coupling phenomena and can be used to elucidate the somewhat obscure macroscopic constitutive behavior of the medium. The two-scale model was discretized by the finite element method. Numerical results were presented in a particular example concerning contaminant migration through a compacted clay liner underneath a sanitary landfill. A particular stratified arrangement for the clay was considered where the unit cell problems were solved analytically when the electric potential is governed by the linearized Poisson–Boltzmann problem. Numerical simulations illustrate the relevance of the two-scale approach to improve the prediction of consolidation of chemically sensitive materials and their relation with the pore-scale behavior. Clearly this provides new insight in the constitutive theory of expansive porous media.

Further work is required to extend the model to media characterized by two levels of porosity (micro- and macro-pores) where the movement of the bulk phase water in the macro-pores is also included. This can be accomplished within the framework of a three-scale approach where an additional level of averaging is required to incorporate the bulk fluid (see e.g. Hueckel et al., 2001). It has been shown by Murad and Cushman (1997, 2000) and Murad et al. (2001) that the development of three-scale models lead to homogenized microstructure models of dual porosity type for deformable porous media where the two-scale homogenized system exchanges mass and momentum with the bulk fluid in the macro-pores. Finally, still within the applications of two-scale models other examples can be pursued such as the sensitivity analysis of the stability of the micro-pores with the reduction in the dielectric constant of the solvent when water is replaced by hydrocarbons. The work of Fernandez and Quigley (1985) provides a comprehensive experimental framework which can be exploited to validate the theory proposed herein. These relevant aforementioned issues will be subject of future work.

Acknowledgements

CM and MM were partly supported by the funding provided by the Lorraine region and the CNPq-CNRS international cooperation agreement. MM would like to acknowledge other related support provided by FAPERJ (Projeto Cientistas do Nosso Estado).

Appendix A. Stratified clay microstructure composed of parallel particles

In this Appendix we present the analytical solutions of the micromechanics (71) and (72) in the case of a stratified clay microstructure composed of parallel particles, when the local electric potential $\overline{\varphi}^0$ is governed by the linearized Poisson–Boltzmann problem.

A.1. Debye–Hueckel approximation

Denoting $\boldsymbol{n}$ and $\boldsymbol{t}$ the unitary vectors normal and tangential to the parallel particles, the microscopic electric field acts normal to the solid, i.e. $\boldsymbol{E}^0 = E_n^0 \boldsymbol{n}$. Assuming the range of low electric potentials $|\overline{\varphi}^0| \ll 1$, the exponential terms in the r.h.s. of (47) can be linearized leading to the well known Debye–Huckel approximation. Denoting $\overline{E}_n^0 = FE_n^0/RT$, the one-dimensional version of the linearized Poisson–Boltzmann problem (47), (posed in the interlayer spacing $-H(x) < y < H(x)$), reads (see Hunter, 1994; Olphen, 1977).

$$\begin{cases} \dfrac{\mathrm{d}^2\overline{\varphi}^0}{\mathrm{d}y^2} = \dfrac{\overline{\varphi}^0}{L_{\mathrm{D}}^2}, \quad \overline{E}_n^0 = -\dfrac{\mathrm{d}\overline{\varphi}^0}{\mathrm{d}y}, \\ \overline{E}_n^0 = 0 \quad \text{at } y = 0, \\ \overline{E}_n^0 = -\dfrac{\sigma F}{\tilde{\varepsilon}\tilde{\varepsilon}_0 RT} \quad \text{at } y = H, \end{cases} \tag{A.1}$$

where $L_{\mathrm{D}} = \left(\tilde{\varepsilon}\tilde{\varepsilon}_0 RT/(2F^2 c_{\mathrm{b}}^0)\right)^{1/2}$ is the Debye's length. The solution $\{\overline{\varphi}^0, \overline{E}_n^0\}$ is given as:

$$\overline{\varphi}^0 = \frac{\sigma}{2Fc_{\mathrm{b}}^0 L_{\mathrm{D}}} \frac{\cosh(y/L_{\mathrm{D}})}{\sinh(H/L_{\mathrm{D}})}, \qquad \overline{E}_n^0 = -\frac{\sigma}{2Fc_{\mathrm{b}}^0 L_{\mathrm{D}}^2} \frac{\sinh(y/L_{\mathrm{D}})}{\sinh(H/L_{\mathrm{D}})}. \tag{A.2}$$

A.2. Darcy's law

We now derive the analytical expressions for the longitudinal scalar components $\{K_{Px}, K_{Cx}, K_{Ex}\}$ of the coefficients $\{\boldsymbol{K}_P, \boldsymbol{K}_C, \boldsymbol{K}_E\}$ in Darcy's law (59). To this end we consider the one-dimensional version of the Stokes problem (55). Standard arguments commonly used in Poiseuille type flows show that pressure and concentration are constant over the cross section and therefore the fluctuations p_{b}^1, $c_{\mathrm{f}}^{\pm 1}$ and $\boldsymbol{f}^{\pm}$ in the transversal direction vanish. Hence, in terms of the axial velocity $v_x^0(y)$ the one-dimensional version of (56) reads

$$\mu_{\mathrm{f}} \frac{\partial^2 v_x^0}{\partial y^2} - \frac{\partial p_{\mathrm{b}}^0}{\partial x} = 2RT\left(\cosh\overline{\varphi}^0 - 1\right)\frac{\partial c_{\mathrm{b}}^0}{\partial x} - 2RTc_{\mathrm{b}}^0 \sinh\overline{\varphi}^0 \frac{\partial \overline{\psi}^0}{\partial x} = RT(\overline{\varphi}^0)^2 \frac{\partial c_{\mathrm{b}}^0}{\partial x} - \tilde{\varepsilon}\tilde{\varepsilon}_0 \frac{\mathrm{d}^2\varphi^0}{\mathrm{d}y^2}\frac{\partial \psi^0}{\partial x}, \tag{A.3}$$

where the one-dimensional version of the Poisson–Boltzmann (47) has been used and the exponential in the first term in the r.h.s. has been linearized up to second order. Denoting $u_x^0(x,t)$ the x-component of the solid displacement, the above problem is supplemented by the boundary conditions $v_x^0(y = H) = \partial u_x^0/\partial t$ and $(\partial v_x^0/\partial y)(y = 0) = 0$. By averaging (A.3) over the cross section, the coefficient $K_{Px} = H^2/3\mu_{\mathrm{f}}$ is the averaged relative velocity $\langle v_x^0 - \partial u_x^0/\partial t\rangle$ with $\partial p_{\mathrm{b}}^0/\partial x = -1$ and $\partial c_{\mathrm{b}}^0/\partial x = \partial \psi^0/\partial x = 0$. Furthermore, the chemico-osmotic component K_C is the averaged of the velocity v_x^0 satisfying

$$\mu_{\mathrm{f}} \frac{\partial^2 v_x^0}{\partial y^2} = -RT(\overline{\varphi}^0)^2.$$

Integrating the above result and using (A.2)(a) for $\overline{\varphi}^0$ we obtain

$$K_{Cx} = \frac{\sigma^2 H^2}{2\mu_f \tilde{\varepsilon}\tilde{\varepsilon}_0 c_b^0 \sinh^2(H/L_D)} \left\{ \frac{1}{6} + \frac{L_D^2}{8H^2} \left[\cosh\left(\frac{2H}{L_D}\right) - \frac{L_D}{2H} \sinh\left(\frac{2H}{L_D}\right) \right] \right\}. \tag{A.4}$$

Finally, adopting the same procedure, the electro-osmotic permeability K_E is the averaged of the velocity component satisfying

$$\mu_f \frac{\partial^2 v_x^0}{\partial y^2} = \tilde{\varepsilon}\tilde{\varepsilon}_0 \frac{d^2\varphi^0}{dy^2} = \frac{\tilde{\varepsilon}\tilde{\varepsilon}_0 RT}{F} \frac{d^2\overline{\varphi}^0}{dy^2}$$

in which after integrating twice and making use of the symmetry at $y = 0$ and no-slip condition at $y = H$ gives

$$\mu_f \frac{\partial v_x^0}{\partial y} = \frac{\tilde{\varepsilon}\tilde{\varepsilon}_0 RT}{F} \frac{d\overline{\varphi}^0}{dy}, \qquad v_x^0(y) = \frac{\tilde{\varepsilon}\tilde{\varepsilon}_0 RT}{\mu_f F} (\overline{\varphi}^0(y) - \overline{\varphi}^0(H)).$$

Hence, after averaging and using (A.2)(a) we have

$$\frac{1}{H} \int_0^H v_x^0 \, dy = \frac{\tilde{\varepsilon}\tilde{\varepsilon}_0 RT}{H\mu_f F} \int_0^H (\overline{\varphi}^0(y) - \overline{\varphi}^0(H)) \, dy = \frac{\tilde{\varepsilon}\tilde{\varepsilon}_0 RT\sigma}{2c_b^0 F^2 \mu_f H} \left(1 - \frac{1}{L_D} \coth\left(\frac{H}{L_D}\right) H \right) \tag{A.5}$$

which yields

$$K_{Ex} = \frac{\sigma L_D}{\mu_f} \left[\frac{L_D}{H} - \coth\left(\frac{H}{L_D}\right) \right]. \tag{A.6}$$

The one-dimensional solutions discussed here resemble in form those presented in e.g. Gross and Osterlé (1968), Fair and Osterlé (1971), Sasidhar and Ruckenstein (1981, 1982) and Yang and Li (1998). Further, denoting $\zeta = \varphi(H)$ the zeta potential, when the thickness of the e.d.l. is small compared to the interlayer spacing H, the Helmholtz–Smoluchowski model can be recovered from (A.6). Under this assumption the first term in the integral in (A.5) involving $\overline{\varphi}^0(y)$ is neglected compared to the second. We then have

$$K_{Ex} = \frac{\tilde{\varepsilon}\tilde{\varepsilon}_0 RT}{H\mu_f F} \int_0^H \overline{\varphi}^0(H) \, dy = \frac{\tilde{\varepsilon}\tilde{\varepsilon}_0 RT}{\mu_f F} \overline{\varphi}^0(H) = \frac{\tilde{\varepsilon}\tilde{\varepsilon}_0 \zeta}{\mu_f} \tag{A.7}$$

which is nothing but the Smoluchowski formula (Hunter, 1981; Coelho et al., 1996; Shang, 1997).

A.3. Movement of the ions

We now derive the one-dimensional linear version of the homogenized diffusion equations (52). To this end denote $\mathscr{D}_{\pm x}^*$ the scalar longitudinal diffusion coefficients and define $\alpha = -\langle \overline{\varphi}^0 \rangle^f = -\sigma/2Fc_b^0 H$. Setting $f^+ = f^- = 0$ in (71) and linearizing the exponential in the homogenized diffusion coefficient we obtain

$$D_{\pm x}^* = D_{\pm x} \langle \exp(\mp \overline{\varphi}^0) \rangle^f \approx D_{\pm}(1 \pm \alpha).$$

Thus, the linearized one-dimensional form of (52) reads

$$\frac{\partial}{\partial t} \left[n_f c_b^0 (1 \pm \alpha) \right] = \frac{\partial}{\partial x} \left[n_f D_{\pm} (1 \pm \alpha) \left(\frac{\partial c_b^0}{\partial x} \pm c_b^0 \frac{\partial \overline{\psi}^0}{\partial x} \right) \right]. \tag{A.8}$$

A.4. Electroneutrality condition

In the case of a stratified microstructure, further consequences of the electroneutrality condition (48) combined with charge conservation (54) can be explored to eliminate the streaming potential in terms of the bulk concentration in both Darcy's law and the diffusion equation. The one-dimensional form of (55) reads

$$n_{\mathrm{f}}\frac{\partial\langle q^0\rangle^f}{\partial t}+\frac{\partial J^0}{\partial x}=0.$$

By combining the above result with the local electroneutrality condition (48) (with σ constant) leads to $\partial J^0/\partial x=0$. Further, together with the homogeneous boundary conditions for the electric current in (73) this yields $J^0=0$. Using this result in the one-dimensional linearized form of (53) we get

$$N^+-N^-=0 \quad \text{with } N^{\pm}=Fn_{\mathrm{f}}D_+(1\pm\alpha)\left(\frac{\partial c_{\mathrm{b}}^0}{\partial x}\pm c_{\mathrm{b}}^0\frac{\partial\overline{\psi}^0}{\partial x}\right).$$

The above constraint leads to the following relation between the gradients of the bulk concentration and streaming potential

$$\frac{\partial\overline{\psi}^0}{\partial x}=-\frac{(1+\alpha)D_+-(1-\alpha)D_-}{(1+\alpha)D_++(1-\alpha)D_-}\,\frac{1}{c_{\mathrm{b}}^0}\,\frac{\partial c_{\mathrm{b}}^0}{\partial x} \tag{A.9}$$

in which when combined with (A.8) and adding the result over cations and anions leads to

$$\frac{\partial}{\partial t}\left(n_{\mathrm{f}}c_{\mathrm{b}}^0\right)=2\frac{\partial}{\partial x}\left[n_{\mathrm{f}}\frac{(1+\alpha)(1-\alpha)D_+D_-}{(1+\alpha)D_++(1-\alpha)D_-}\,\frac{\partial c_{\mathrm{b}}^0}{\partial x}\right]. \tag{A.10}$$

Further, the same procedure can be adopted to eliminate the electro-osmotic component in the one-dimensional form of Darcy's law. This yields

$$\left\langle v_x^0\right\rangle^f=-K_P\frac{\partial p_{\mathrm{b}}^0}{\partial x}-K_C^{\mathrm{eff}}\frac{\partial c_{\mathrm{b}}^0}{\partial x} \tag{A.11}$$

with

$$K_C^{\mathrm{eff}}\equiv K_C-K_E\frac{1}{c_{\mathrm{b}}^0}\,\frac{(1+\alpha)D_+-(1-\alpha)D_-}{(1+\alpha)D_++(1-\alpha)D_-}. \tag{A.12}$$

It should be noted that the sign of the effective osmotic coefficient K_C^{eff} may change according to the magnitude of the terms in the r.h.s. of (A.12). In the flow regime characterized by $K_C^{\mathrm{eff}}>0$, the chemical component of the filtration velocity is dictated by the so-called anomalous (reverse) osmosis which follows the negative of the concentration gradient. Conversely, when the electro-osmotic component (last term in the r.h.s. of (A.12)) prevails, flow is governed by a regular osmosis process, following the concentration gradient.

A.5. Modified Terzaghi's decomposition

We now derive a sharper representation for the modified Terzaghi's decomposition (67) in the particular case of stratified microstructure. From (27)(b) and (62) the reduced representations of $\boldsymbol{\tau}_{\mathbf{M}}^0$ and $\boldsymbol{\Pi}_d^0$ are

$$\begin{aligned}\boldsymbol{\tau}_{\mathrm{M}}^0&=\frac{\tilde{\varepsilon}\tilde{\varepsilon}_0}{2}\left((E_n^0)^2\boldsymbol{n}\otimes\boldsymbol{n}-(E_n^0)^2\boldsymbol{t}\otimes\boldsymbol{t}\right),\\ \boldsymbol{\Pi}_d^0&=\left(\pi^0-\frac{\tilde{\varepsilon}\tilde{\varepsilon}_0}{2}(E_n^0)^2\right)\boldsymbol{n}\otimes\boldsymbol{n}+\left(\pi^0+\frac{\tilde{\varepsilon}\tilde{\varepsilon}_0}{2}(E_n^0)^2\right)\boldsymbol{t}\otimes\boldsymbol{t}.\end{aligned} \tag{A.13}$$

The electrostatic component of the disjoining pressure Π_d^0 is defined as the projection of $\boldsymbol{\Pi}_d^0\boldsymbol{n}$ onto the normal direction to the solid phase, i.e. $\Pi_d^0\equiv\boldsymbol{\Pi}_d^0\boldsymbol{n}\cdot\boldsymbol{n}$ (Derjaguin et al., 1987). We then have

$$\boldsymbol{\Pi}_d^0=\Pi_d^0\boldsymbol{n}\otimes\boldsymbol{n}+\left(\Pi_d^0+\tilde{\varepsilon}\tilde{\varepsilon}_0(E_n^0)^2\right)\boldsymbol{t}\otimes\boldsymbol{t} \tag{A.14}$$

in which when combined with (16) and (A.2) and linearizing up to second order gives

$$\begin{aligned}\Pi_d^0 &= \pi^0 - \frac{\tilde{\varepsilon}\tilde{\varepsilon}_0}{2}(E_n^0)^2 = 2RTc_{\mathrm{b}}^0\big(\cosh\overline{\varphi}^0 - 1\big) - \frac{\tilde{\varepsilon}\tilde{\varepsilon}_0}{2}(E_n^0)^2 \\ &\approx RTc_{\mathrm{b}}^0(\overline{\varphi}^0)^2 - \frac{\tilde{\varepsilon}\tilde{\varepsilon}_0(RT)^2}{2F^2}(\overline{E}_n^0)^2 \\ &= \frac{RT\sigma^2}{4F^2c_{\mathrm{b}}^0L_{\mathrm{D}}^2\sinh^2(H/L_{\mathrm{D}})}\left[\cosh^2\left(\frac{y}{L_{\mathrm{D}}}\right) - \frac{\tilde{\varepsilon}\tilde{\varepsilon}_0RT}{2F^2c_{\mathrm{b}}^0L_{\mathrm{D}}^2}\sinh^2\left(\frac{y}{L_{\mathrm{D}}}\right)\right] \\ &= \frac{RT\sigma^2}{4F^2c_{\mathrm{b}}^0L_{\mathrm{D}}^2\sinh^2(H/L_{\mathrm{D}})} = \frac{\sigma^2}{2\tilde{\varepsilon}\tilde{\varepsilon}_0\sinh^2(H/L_{\mathrm{D}})}.\end{aligned} \tag{A.15}$$

The above equation reproduces the well known result of the e.d.l. where Π_d^0 is constant in the interlayer spacing. Further, applying (A.13) to the normal and using (A.15), the traction boundary condition in the cell problem (65) for $\boldsymbol{u}_\pi^1$ reduces to $\boldsymbol{c}_{\mathrm{s}}\mathscr{E}_y(\boldsymbol{u}_\pi^1)\boldsymbol{n} = -\Pi_d^0\boldsymbol{n}$ (constant). Recalling definition (68)(b) for $\boldsymbol{\Pi}_S^0$, the averaged solution of (65) for the parallel particle arrangement is $\boldsymbol{\Pi}_S^0 = \Pi_d^0\boldsymbol{n}\otimes\boldsymbol{n}$. Thus, defining for swelling pressure Π_S^0 as the projection $\Pi_S^0 \equiv \boldsymbol{\Pi}_S^0\boldsymbol{n}\cdot\boldsymbol{n}$ this yields $\Pi_S^0 = \Pi_d^0$. It remains to obtain the physical interpretation of the tangential component of the tensor $\boldsymbol{\Pi}_d^0$ in (A.14). To this end we combine this result with the constitutive law $\boldsymbol{\sigma}_{\mathrm{f}}^0 = -p^0\boldsymbol{I} + \boldsymbol{\tau}_{\mathrm{M}}^0 = -(p_{\mathrm{b}}^0 + \pi^0)\boldsymbol{I} + \boldsymbol{\tau}_{\mathrm{M}}^0 = -p_{\mathrm{b}}^0\boldsymbol{I} - \boldsymbol{\Pi}_d^0$ to obtain

$$\boldsymbol{\sigma}_{\mathrm{f}}^0 = -p_n^0\boldsymbol{n}\otimes\boldsymbol{n} - p_t^0\boldsymbol{t}\otimes\boldsymbol{t}$$

with the normal and tangential components given as

$$p_n^0 = p_{\mathrm{b}}^0 + \Pi_d^0, \qquad p_t^0 = p_{\mathrm{b}}^0 + \Pi_d^0 + \tilde{\varepsilon}\tilde{\varepsilon}_0(E_n^0)^2.$$

The interfacial tension of the electrolyte solution γ_{fs} is defined as the excess quantity (see e.g. Toshev and Ivanov, 1975)

$$\gamma_{\mathrm{fs}}^0 = -\int_{-H}^{H}(p_t^0 - p_{\mathrm{b}}^0)\,\mathrm{d}h = -\int_{-H}^{H}(p_t^0 - p_n^0)\,\mathrm{d}h - \int_{-H}^{H}(p_n^0 - p_{\mathrm{b}}^0)\,\mathrm{d}h = -\tilde{\varepsilon}\tilde{\varepsilon}_0\int_{-H}^{H}(E_n^0)^2\,\mathrm{d}h - \int_{-H}^{H}\Pi_d^0\,\mathrm{d}h. \tag{A.16}$$

Denote A the total surface area of the particles within each unit cell and $a_{\mathrm{fs}} \equiv |A|/|Y|$ the specific area density per unit volume. Using (A.16) in (A.14), the averaged disjoining tensor $\langle\boldsymbol{\Pi}_d^0\rangle$ can be represented as (recall that $\Pi_d^0 = \Pi_S^0 = \text{constant}$)

$$\langle\boldsymbol{\Pi}_d^0\rangle = n_{\mathrm{f}}\Pi_S^0\boldsymbol{n}\otimes\boldsymbol{n} - a_{\mathrm{fs}}\gamma_{\mathrm{fs}}\boldsymbol{t}\otimes\boldsymbol{t}. \tag{A.17}$$

Hence, the macroscopic physico-chemical tensor $\boldsymbol{\Pi}^0$ in (68) can be represented as

$$\boldsymbol{\Pi}^0 = n_{\mathrm{s}}\boldsymbol{\Pi}_S^0 + \langle\boldsymbol{\Pi}_d^0\rangle = \Pi_S^0\boldsymbol{n}\otimes\boldsymbol{n} - a_{\mathrm{fs}}\gamma_{\mathrm{fs}}\boldsymbol{t}\otimes\boldsymbol{t}. \tag{A.18}$$

The above representation for $\boldsymbol{\Pi}^0$ in the stratified arrangement aims at decomposing this quantity into two components acting normal and tangential to the solid surface. In contrast to the tangential component $a_{\mathrm{fs}}\gamma_{\mathrm{fs}}\boldsymbol{t}\otimes\boldsymbol{t}$, the normal one $\Pi_S^0\boldsymbol{n}\otimes\boldsymbol{n}$ is an effective quantity as it is directly responsible for the expansion/shrinking of the particles. Thus, when combined with (67) the decomposition (A.18) furnishes an alternative form of expressing the modified Terzaghi's principle wherein physico-chemical stresses appear decomposed explicitly into their effective and non-effective components.

Appendix B. Dimensionless unknowns

In the analysis that follows we rewrite the previous one-dimensional system applied to the clay liner example in dimensionless form. The corresponding dimensionless variables are defined relative to reference quantities. Denoting the former set by the superscript $*$ and the latter by the subscript ref, we then have e.g. $c_{\mathrm{b}}^{*} = c_{\mathrm{b}}^{0}/c_{\mathrm{ref}}$, $p_{\mathrm{b}}^{*} = p_{\mathrm{b}}^{0}/p_{\mathrm{ref}}$, $\Pi^{*} = \Pi_{S}^{0}/p_{\mathrm{ref}}$. To simplify the following notation and reduce the number of subscripts, the longitudinal component of a vectorial quantity is denoted with the same symbol of the corresponding vector (or tensor) without the boldface. For the clay liner example the reference values $\{c_{\mathrm{ref}}, p_{\mathrm{ref}}\}$ are selected as the components which appear in the non-homogeneous boundary conditions (73) on Γ_1, i.e. $c_{\mathrm{ref}} = c_{*}$ and $p_{\mathrm{ref}} = h$. The dimensionless streaming potential is defined as $\psi^{*} = \overline{\psi} = F\psi_0/RT$. In addition, the dimensionless macroscopic coordinates are defined as $x^{*} = x/L_{\mathrm{ref}}$ and $y^{*} = y/L_{\mathrm{ref}}$, where L_{ref} is chosen as the macroscopic height of the liner $L_{\mathrm{ref}} = L_0$. Also the reference interlayer spacing H_{ref} is chosen of the value of H initially before the chemo-mechanical consolidation. Whence, the reference hydraulic conductivity is given as $K_{\mathrm{Pref}} = H_{\mathrm{ref}}^{2}/3\mu_{\mathrm{f}}$. Further, defining the dimensionless time $t^{*} = (\lambda + 2\mu)K_{\mathrm{Pref}}t/L_{\mathrm{ref}}^{2}$ and the longitudinal components of the Darcy velocity and solid displacement as $v_{\mathrm{D}}^{*} = v_{\mathrm{D}}^{0}L_{\mathrm{ref}}/(K_{\mathrm{Pref}}p_{\mathrm{ref}})$ and $u^{*} = u(\lambda_{\mathrm{s}} + 2\mu_{\mathrm{s}})/p_{\mathrm{ref}}L_{\mathrm{ref}}$, the unidimensional dimensionless forms of Darcy's law along with overall mass balance and equilibrium condition read

$$\begin{aligned} v_{\mathrm{D}}^{*} &= -K_{P}^{*}\frac{\partial p_{\mathrm{b}}^{*}}{\partial x^{*}} - K_{C}^{*}\frac{\partial c_{\mathrm{b}}^{*}}{\partial x^{*}}, \\ \frac{\partial v_{\mathrm{D}}^{*}}{\partial x^{*}} &+ \frac{\partial^{2}u^{*}}{\partial t^{*}\partial x^{*}} = 0, \\ \frac{\partial^{2}u^{*}}{\partial x^{*2}} &- \frac{\partial p_{\mathrm{b}}^{*}}{\partial x^{*}} = 0, \end{aligned} \tag{B.1}$$

where

$$K_{P}^{*} = \frac{K_{P}}{K_{\mathrm{Pref}}}, \qquad K_{C}^{*} = \frac{c_{\mathrm{ref}}K_{C}^{\mathrm{eff}}}{K_{\mathrm{Pref}}p_{\mathrm{ref}}}.$$

In the last equation in (B.1), the effects of the disjoining pressure were not included as it only acts in the transversal direction in the stratified arrangement. Finally, the dimensionless ion diffusion equation (A.10) is given by

$$\frac{\partial(n_{\mathrm{f}}c^{*})}{\partial t^{*}} = \frac{\partial}{\partial x^{*}}\left(n_{\mathrm{f}}D^{*}\frac{\partial c^{*}}{\partial x^{*}}\right)$$

with

$$D^{*} = \frac{1}{K_{\mathrm{Pref}}\,p_{\mathrm{ref}}(\lambda + 2\mu)}\left[2\frac{(1+\alpha)(1-\alpha)D_{+}\mathscr{D}_{-}}{(1+\alpha)D_{+} + (1-\alpha)D_{-}}\right].$$

References

Anandarajah, A., 1997. Influence of particle orientation on one-dimensional compression of montmorillonite. J. Colloid Interf. Sci. 194, 44–52.

Auriault, J., 1991. Heterogeneous media: Is an equivalent homogeneous description always possible? Int. J. Engrg. Sci. 29, 785–795.

Auriault, J., Adler, P., 1995. Taylor dispersion in porous media: Analysis by multiple scale expansions. Adv. Water Res. 18 (4), 217–226.

Auriault, J., Sanchez-Palencia, E., 1977. Etude du comportement macroscopique d'un milieu poreux saturé déformable. J. Mecanique 16 (4), 575–603.

Auriault, J.L., 1990. Geomaterials: Constitutive Equations and Modeling. In: Darve, F. (Ed.), Elsevier, New York, Ch. Behavior of porous saturated deformable media, pp. 311–328.
Barbour, S., Fredlund, D., 1989. Mechanisms of osmotic flow and volume changes in clay soils. Can. Geotech. J. 26, 551–562.
Bennethum, L., Murad, M.A., Cushman, J., 2000. Macroscale thermodynamics and the chemical potential for swelling porous media. Transport Porous Med. 39, 187–225.
Bike, S., Prieve, C., 1992. Electrohydrodynamics of thin double layers: A model for the streaming potential profile. J. Colloid Interf. Sci. 154 (1), 87–96.
Biot, M., Willis, D.G., 1957. The elastic coefficients of the theory of consolidation. J. Appl. Mech. 79, 594–601.
Callen, H., 1985. Thermodynamics and an Introduction to Thermostatics. Wiley, New York.
Coelho, D., Shapiro, M., Thovert, J., Adler, P., 1996. Electroosmotic phenomena in porous media. J. Colloid Interf. Sci. 181, 169–190.
Dahnert, K., Huster, D., 1999. Comparison of the Poisson–Boltzmann model and the donnan equilibrium of a polyelectrolyte in salt solution. J. Colloid Interf. Sci. 215, 131–139.
Derjaguin, B.V., Churaev, N., Muller, V., 1987. Surface Forces. Plenum Press, New York.
Donnan, F., 1924. The theory of membrane equilibria. Chem. Rev. 1, 73–90.
Eringen, A., Maugin, G., 1989. Electrodynamics of Continua. Springer-Verlag.
Fair, J.C., Osterlé, J.F., 1971. Reverse electrodialysis in charged capillary membranes. J. Chem. Phys. 54 (8), 3307–3316.
Fernandez, F., Quigley, R., 1985. Hydraulic conductivity of natural clays permeated with simple hydrocarbons. Can. Geotech. J. 22, 205–214.
Gross, R.J., Osterlé, J.F., 1968. Membrane transport characteristics of ultrafine capillaries. J. Chem. Phys. 49 (1), 228–234.
Gu, W., Lai, W., Mow, V., 1998a. A mixture theory for charged–hydrated soft tissues containing multi-electrolytes: Passive transport and swelling behaviors. J. Biomech. Engrg. 120, 169–180.
Gu, W., Lai, W., Mow, V., 1998b. A triphasic analysis of negative osmotic flows through charged hydrated tissues. J. Biomech. 30 (1), 71–78.
Heidug, W., Wong, S., 1996. Hydration swelling of water-adsorbing rocks: A constitutive model. Int. J. Numer. Anal. Meth. Geomech. 20, 403–430.
Hueckel, T., 1992a. On effective stress concepts and deformation in clays subjected to environmental loads. Can. Geotech. J. 29, 1120–1125.
Hueckel, T., 1992b. Water mineral interaction in hygromechanics of clays exposed to environmental loads: a mixture theory approach. Can. Geotech. J. 29, 1071–1086.
Hueckel, T., Loret, B., Gajo, A., 2001. Proceedings of the Workshop on Clay behavior; Chemo-Mechanical coupling, Maratea. Di Maio, T. Hueckel B. Loret, Ch. Swelling materials as reactive, deformable, two-phase continua: Basic modeling concepts and options, pp. 121–133.
Hunter, R., 1981. Zeta Potential in Colloid Science: Principles and Applications. Academic Press, New York.
Hunter, R., 1994. Introduction to Modern Colloid Science. Oxford University Press, Oxford.
Huyghe, J., Janssen, J., 1997. Quadriphasic mechanics of swelling incompressible porous media. Int. J. Engrg. Sci. 25 (8), 793–802.
Israelachvili, J., 1991. Intermolecular and Surfaces Forces. Academic Press, New York.
Kaczmarek, M., Hueckel, T., 1998. Chemo-mechanical consolidation of clays: Analytical solutions for a linearized one-dimensional problem. Transport Porous Med. 32, 49–74.
Kim, D.J., Diels, J., Feyen, J., 1992. Water movement associated with overburden potential in a shrinking marine clay soil. J. Hydrol. 133, 179–200.
Lai, W., Hou, J., Mow, V., 1991. A triphasic theory for the swelling and deformation behaviors of articular cartilage. J. Biomech. Engrg. 113, 245–258.
Lambe, T.W., 1960. A mechanistic picture of shear strength in clay. In: Proceedings of the ASCE research conference on shear strength of cohesive soils, Boulder Colorado, pp. 503–532.
Landau, L., Lifshitz, E., 1960. Electrodynamics of Continuous Media. Pergamon Press, Oxford.
Levenston, M., Eisenberg, S., Grodzinsky, A., 1998. A variational formulation for coupled physicochemical flows during finite deformation of charged porous media. Int. J. Solids Struct. 35 (34-35), 4999–5019.
Low, P., 1987. Structural component of the swelling pressure of clays. Langmuir 3, 18–25.
Lydzba, D., Shao, J., 2000. Study of poroelasticity material coefficients as response of microstructure. Mech. Cohes.-Frict. Mater. 5, 149–171.
Lyklema, J., 1993. Fundamentals of Colloid and Interface Science. Academic Press, London.
Mow, V., Ateshian, A., Lai, W., Gu, W., 1998. Effects of fixed charges on the stress-relaxation behavior of hydrated soft tissues in a confined compression problem. Int. J. Solids Struct. 35 (34–35), 4945–4962.
Moyne, C., Murad, M., 1999. Proceedings of the IUTAM Symposium on Theoretical and Numerical Methods in Continuum Mechanics of Porous Materials, Stuttgart, w. elhers Edition. Kluwer, Ch. Macroscopic swelling of clays derived from homogenization, pp. 329–334.

Moyne, C., Murad, M., in press. Macroscopic behavior of swelling porous media derived from micromechanical analysis. Transport Porous Med.

Murad, M., 1999. A thermomechanical model of hydration swelling in smectite clays, i. two-scale mixture-theory approach. Int. J. Numer. Anal. Meth. Geomech. 23 (7), 673–696.

Murad, M., Cushman, J., 1997. A multiscale theory of swelling porous media: II. dual porosity models for consolidation of clays incorporating physicochemical effects. Transport Porous Med. 28 (1), 69–108.

Murad, M., Cushman, J., 2000. Thermomechanical theories for swelling porous media with microstructure. Int. J. Engrg. Sci. 38 (5), 517–564.

Murad, M., Guerreiro, J., Loula, A.F., 2001. Micromechanical computational modeling of secondary consolidation and hereditary creep in soils. Comput. Meth. Appl. Mech. Engng. 190 (15), 1985–2016.

Olphen, V., 1977. An Introduction to Clay Colloid Chemistry: For Clay Technologists, Geologists, and Soil Scientists. Wiley, New York.

Philip, J., 1969. Hydrostatics and hydrodynamics in swelling soils. Water Resour. Res. 143, 1070–1077.

Ren, L., Li, D., Qu, M., 2001. Electro-viscous effects on liquid flow in microchannels. J. Colloid Interf. Sci. 233, 12–22.

Samson, E., Marchand, J., Robert, J., Bournazel, J., 1999. Modeling ion diffusion mechanisms in porous media. Int. J. Numer. Meth. Engrg. 46, 2043–2060.

Sanchez-Palencia, E., 1980. Non-Homogeneous Media and Vibration Theory. Lectures Notes in Physics. Springer Verlag.

Sasidhar, V., Ruckenstein, E., 1981. Electrolyte osmosis through capillaries. J. Colloid Interf. Sci. 82 (2), 439–457.

Sasidhar, V., Ruckenstein, E., 1982. Anomalous effects during electrolyte osmosis across charged porous membranes. J. Colloid Interf. Sci. 85 (2), 332–361.

Shang, J., 1997. Zeta potential and electroosmotic permeability of clay soils. Can. Geotech. J. 34, 627–631.

Sherwood, J., Rubio-Hernandez, F., Ruiz-Reina, E., 2000. The primary electroviscous effect: Thin double layers and a stern layer. J. Colloid Interf. Sci. 228, 7–13.

Smiles, D., Rosenthal, M.J., 1968. The movement of water in swelling materials. Aust. J. Soil. Res. 6, 237–248.

Smith, D., 1999. One-dimensional contaminant transport through a deforming porous medium. Int. J. Numer. Anal. Meth. Geomech. 24 (8), 693–722.

Sridharan, A., Rao, G., 1973. Controlling volume change of saturated clays and the role of the effective stress concept. Geotechnique 23 (3), 359–382.

Terada, K., Ito, T., Kikuchi, N., 1998. Characterization of the mechanical behaviors of solid–fluid mixture by the homogenization method. Comput. Meth. Appl. Mech. Engrg. 153, 223–257.

Toshev, B., Ivanov, I., 1975. Thermodynamics of thinliquid films i: Basic relations and conditions of equilibrium. Colloid Polym. Sci. 253, 558–565.

Whitaker, S., 1999. The Method of Volume Averaging. Theory and Applications of Transport in Porous Media. Kluwer Academic publishers.

Yang, C., Li, D., 1998. Analysis of electrokinetic effects on the liquid flow in rectangular microchannels. Colloid Surf. A 143, 339–353.

Zhou, Y., Rajapakse, R., Graham, J., 1998. A coupled thermoporoelastic model with thermo-osmosis and thermal-filtration. Int. J. Solids Struct. 35 (34–35), 4659–4683.